

Manuscript Number: JFUE-D-17-02705R1

Title: Experiments and Modeling of the Autoignition of Methyl Pentanoate at Low to Intermediate Temperatures and Elevated Pressures in a Rapid Compression Machine

Article Type: Research paper

Keywords: chemical kinetics, rapid compression machine, autoignition, methyl ester, methyl valerate, methyl pentanoate

Corresponding Author: Dr. Bryan W Weber,

Corresponding Author's Institution: University of Connecticut

First Author: Bryan W Weber

Order of Authors: Bryan W Weber; Justin A Bunnell, M.S.; Kamal Kumar, Ph.D.; Chih-Jen Sung, Ph.D.

Abstract: Methyl valerate ($C_6H_{12}O_2$, methyl pentanoate) is a methyl ester and a relevant surrogate component for biodiesel. In this work, we present ignition delays of methyl valerate measured using a rapid compression machine at a range of engine-relevant temperature, pressure, and equivalence ratio conditions. The conditions we have studied include equivalence ratios (ϕ) from 0.25 to 2.0, temperatures between 680 K and 1050 K, and pressures of 15 bar and 30 bar. The ignition delay data demonstrate a negative temperature coefficient region in the temperature range of 720 K-800 K for both $\phi = 2.0$, 15 bar and $\phi = 1.0$, 30 bar, with two-stage ignition apparent over the narrower temperature ranges of 720 K-760 K for 15 bar and 740 K-760 K at 30 bar. In addition, the experimental ignition delay data are compared with simulations using an existing chemical kinetic model from the literature. The simulations with the literature model under-predict the data by factors between 2 and 10 over the entire range of the experimental data. In addition, a new chemical kinetic model is developed using the Reaction Mechanism Generator (RMG) software. The agreement between the experimental data and the RMG model is also not satisfactory. To help determine the possible reasons for the disagreement, a path analysis of both models is completed. It is found that improvements to both the reaction pathways and thermodynamic properties are required. Further directions for future improvement of the methyl valerate model are discussed.

Bryan W. Weber
Department of Mechanical Engineering
University of Connecticut
191 Auditorium Road U-3139
Storrs, CT 06269-3139

September 27, 2017

Dear Prof. Suuberg,

Thank you for sending us the comments of the reviewers. We have considered each of the comments individually, and prepared a detailed response, as well as the revised manuscript. In addition, we have attached a marked copy showing the added and deleted text. We look forward to your decision on the manuscript.

Thank you again for your consideration of this manuscript.

Sincerely,

Bryan W. Weber

Experiments and Modeling of the Autoignition of Methyl Pentanoate at Low to Intermediate Temperatures and Elevated Pressures in a Rapid Compression Machine
Ms. Ref. No.: JFUE-D-17-02705

We would like to thank the reviewers for their thoughtful comments. Below are detailed responses to each of the reviewers' comments. In the attached marked revision, deleted text is marked in red and added text is marked in blue.

Reviewer #1:

Reviewer: *The authors study ignition of methyl pentanoate, a small methyl ester, in the current study. The data from the current study is helpful in establishing the reaction rates which can be systematically used for developing the kinetic models for large esters and hence very valuable for developing kinetic models of biodiesel. The study also shows the poor performance of the literature models in estimating the ignition delays underscoring the need for such novel experimental datasets and hence would recommend this work for publication. However, I think the manuscript needs to be revised before it can be published. Below are the specific comments which I think need to be addressed before it can be published.*

Our Response: Thank you for your comments. Detailed responses to each comment are below.

Reviewer: *Please improving the quality of figures. For eg: First stage and total ignition delay Symbols in Figs 5a & 5b are very hard to differentiate. Figure 1 could also be improved.*

Our Response: We have increased the mark size on Fig. 5 to better distinguish the overall ignition delay and the first-stage ignition delay. On Fig. 1, we made several changes to improve the clarity, including swapping the colors of reactive and non-reactive pressure traces, changing the non-reactive pressure to a dashed line style, and making the black lines thinner.

Reviewer: *Regarding the statement "The NTC region of MV is mapped out to provide additional information on the fidelity of using MV as a biodiesel surrogate." I am not convinced that MV could be a biodiesel surrogate, in my opinion it helps in understanding the chemistry of large esters.*

Our Response: We agree with the reviewer that it is possible that MV will not be a good surrogate for biodiesel. Nonetheless, to our knowledge, there has been no study to suggest that it is not a good surrogate, probably because very few studies of MV have been conducted to date, so there is not enough information to judge. However, we think that judging the suitability (or lack thereof) for MV as a surrogate of biodiesel is outside the scope of this work, so we are simply noting that this study provides part of the necessary experimental information so that others may judge for themselves. We also agree with the reviewer that the scope of this work is actually wider than we had noted previously, so we have added a note that this study provides further information on the autoignition chemistry of large methyl esters near line 41:

"The NTC region of MV is mapped out to provide additional information on the fidelity of using MV as a biodiesel surrogate and insights into the autoignition chemistry of large methyl esters."

Reviewer: *Specify the units of coefficients B, C and, temperature T in equation (1)*

Our Response: The coefficients are in kPa and K. This has been added to the text near line 112 and in the caption of Table 2.

"... where A, B, and C are substance-specific coefficients, given in units of K and kPa."

Reviewer: *The authors report an ignition delay of 100 ms at 640 K $f=2$, MV/air mixture at 15 bar. So at 30 bar I would expect an ignition delay which is for sure will be more than 10 ms. So I am surprised by the statement "For the $\phi = 2.0$ condition, only $P_C = 15$ bar is considered because we could not achieve*

TC values low enough that the ignition during the compression stroke can be prevented'. Can the authors comment on this.

Our Response: The reason for this is because of physical limitations of the experimental apparatus and the fuel. In particular, achieving sufficiently EOC low temperatures on our apparatus would require increasing the reaction chamber volume at the end of compression, which in turn requires substantially higher initial pressures to reach the EOC pressure of 30 bar. The initial pressure in the RCM reaction chamber is limited by the pressure in the mixing tank, and the total pressure in the mixing tank is limited by the vapor pressure of MV at the preheat temperature. The combination of these factors meant that we could not prepare a mixture with sufficiently high tank pressure to enable repeated experiments with the EOC volume required to reach EOC temperatures where the ignition delay would be measurable. However, we feel that this explanation would only confuse the manuscript, so we omit it.

Reviewer: *The comparison of ignition delays of MV from current work and that of Hadj-Ali et al. [9] would be helpful.*

Our Response: The ignition delays of MV measured in the work of Hadj-Ali et al. [9] were conducted at several pressures and roughly a single EOC temperature (near 815 K). However, none of the pressures considered in that study match the pressures considered in our study, so we feel that including the data on one of our existing plots would be very confusing. Moreover, the influence of facility-specific effects make a direct comparison of ignition delays from different RCMs somewhat challenging, particularly without experimental pressure traces of MV from the work of Hadj-Ali et al. [9] to compare the facility effects. Therefore, we have not added a figure with this comparison.

Reviewer: *On discussion related to Dievart model in figure 5, it is surprising that $\phi=0.25$ and $\phi=0.5$ simulations show NTC but $\phi=1$ and $\phi=2$ simulations do not. The trend is counter intuitive as the cool flame chemistry and NTC response are expected to increase with increase in equivalence ratio. This needs to be clarified. My guess is that the location of the NTC is not captured accurately by model. NTC region predicted by model is shifted to high temperatures where ignition is observed in RCM simulations. Showing Adiabatic constant volume simulations to understand the location of NTC at different equivalence ratios.*

Our Response: We agree with the reviewer that the location of the NTC region with respect to inverse temperature is not well captured by the model. It does seem as though the NTC has been shifted to higher temperatures with respect to the data, in addition to the model being too reactive. This is supported by the newly added Fig. 6, which compares adiabatic, constant volume simulations with the RCM simulations from Fig. 5. It is apparent from this figure that the predicted ignition delays in the $P_C = 15$ bar, $\phi = 2.0$ and the $P_C = 30$ bar, $\phi = 1.0$ simulations fall on the low temperature side of the NTC, while the $P_C = 15$ bar, $\phi = 0.25$ and 0.50 simulated ignition delays are on the high-temperature side of the NTC, but approaching the NTC range such that they start to assume the characteristic curvature as the temperature decreases. In addition to the figure, we have added some paragraphs near line 293 to clarify this point, but we have not copied the added text here to save space.

Reviewer: *Figure 5 caption could also be revised.*

Our Response: We have modified the text of the caption of Fig. 5 to read:

“Comparison of experimental (τ and τ_1) and simulated (τ) ignition delays computed using the procedure described in Section 3.1. a) 15 bar, b) 30 bar.”

Reviewer: *From Figure 5a for $\phi=2$, 15 bar and fig. 5b $\phi=1$, 30 bar the Dievart et al. model consistently under predicts the ignition delays which contradicts the statement "While the model of Dievart et al. [15] over-predicts the first-stage ignition delay, it also over-predicts the first-stage pressure rise, thereby leading to rapid overall ignition." This needs to be revised.*

Our Response: This statement has been removed from the manuscript.

Reviewer: *On discussion related to RMG model from Figure 5, the authors state "model over-predicts the low-temperature ignition delays and does not predict.." define low temperature ignition delays." The ignition delays from RMG model and experiments cross over around 720 K so the statement that low temp. ignition delays are overpredicted is not completely accurate.*

Our Response: In this context, we are defining low temperature ignition delays as those to the right of the experimental NTC region on the Arrhenius plot. We have added the following text near line 319:

“... the RMG model tends to over-predict the low-temperature overall ignition delays (i.e., those to the right of the experimental NTC region on the Arrhenius plot)...”

Reviewer: *Regarding the heat of formation shown in Table 3, it is interesting that the heat of formation of radical 3 and 4 estimated by RMG are different. I would request the authors check their numbers.*

Our Response: We have checked the values for the estimates in the mechanism, and they are identical to the values in Table 3 and further identical to the values available from the RMG website at <http://rmg.mit.edu>. As such, no changes have been made to the manuscript in response to this comment.

Reviewer: *The authors use the branching ratios of fuel decomposition to fuel radicals to state the importance of fuel chemistry in the current work. The relative consumption shown in Table 4 demonstrates that the branching ratios do not exhibit strong sensitive to thermochemistry which is supported by the fact that RMG and RMG switched show nearly identical branching ratios. I am not convinced that the importance of the thermochemistry is elucidated by the current discussion related to Table 4 and the discussion in my opinion does not provide any kinetic insights. May be the discussion could be removed.*

Our Response: We have clarified the discussion of this point. In particular, we have emphasized that the results show that both the thermochemistry and reaction pathways are important, and cannot easily be disentangled from each other, requiring a thorough, detailed investigation of the methyl valerate reaction system which we consider outside the scope of the present work. In addition, we have noted that improper prediction of the thermochemistry of species may affect the RMG-generated model in particular due to the rate-based algorithm used in RMG, which may miss important reactions if the thermochemistry is not accurate. We have modified the text beginning near line 402, but do not copy the modification here for space.

Reviewer: *Alternatively, it would be interesting to compare the thermochemistry of the low temperature chemistry related reactions (RO2 chemistry) from models and ab-initio works like those Hayes and Burgess and also try adopting the reaction rates from ab-initio calculations and see to if the mechanism performance improves.*

Our Response: We feel that the poor performance of both mechanisms indicates that a thorough and detailed study of the entire methyl valerate system is warranted, and small modifications, such as the replacement of only a few rates related to low-temperature chemistry, will not be sufficient to significantly improve the performance of the model. Moreover, we feel that such ad-hoc replacement of rates, even if the performance improves, could not be shown to be anything more than fortuitous without further detailed study, which is outside the scope of the present work. Finally, in a separate work, Diévar et al. (Combustion and Flame, 159 (5) 1793–1805, 2012) note that “preliminary tests with up-to-date kinetic parameters [including the work of Hayes and Burgess] for the generic low temperature scheme have shown an enhancement of the fuel reactivity at the end of the NTC region.” Since the model already over-predicts the reactivity of the RCM data, particularly at the end of the NTC region, further enhancement is not likely to improve agreement.

Therefore, we have not included these modifications in the manuscript; we have, however, added a note to the end of the discussion (near line 418) that references the work of Hayes and Burgess [14] to indicate

that some of the necessary detailed work has been started.

Reviewer #2:

Reviewer: *The measurement of Methyl Valerate at these temperature and pressure conditions constitutes important work and the manuscript of well laid out and has potential to be widely circulated. The arguments in the article are sound and the figures are clear.*

Our Response: Thank you for your comments. A detailed response is below.

Reviewer: *I would like to ask the authors to check one item definitively before the article is published. I am concerned that at these higher pressures and equivalence ratios close to 1, there would be ignition which occurs during the compression stroke. This would not be noticed if some of the fuel condenses during the charging process and thereby you are dealing with lean mixtures than those cited in the paper. The authors are encouraged to make sure this is not the case by possibly sampling the charge after filling through a GC or by a quantitative absorption method as that used routinely by Stanford.*

Our Response: With regards to ignition during the compression stroke, we have compared each reactive pressure trace to its corresponding non-reactive trace and found they are in good agreement from the beginning to the end of compression, indicating that there is no heat release during the compression stroke. With regards to the filling process, we have thoroughly checked the temperatures throughout the apparatus and found them to be quite consistent, including the mixing tanks, the piping connections, and the reaction chamber itself. Moreover, we have conducted several studies in the past utilizing GC to determine mole fractions of components. All of these studies determined that the vaporization procedure used on this apparatus is sufficient to produce a homogeneous mixture of fuel and oxidizer, even for fuels with relatively low vapor pressures. We have added references to these prior studies in the present manuscript near line 110:

“Previous work has shown this procedure to completely vaporize the fuel and prevent fuel cracking during the heating process [25, 26, 27].”

Reviewer: *In the future, a possible direct charging method might be encouraged instead of a mix vessel.*

Our Response: We first note that direct charging methods have their own set of disadvantages, and are still required to address the issues of fuel condensation and fuel-oxidizer mixing. However, we feel that adding a detailed discussion of the advantages and disadvantages of each mixing method to the manuscript would be beyond the scope of the current work, and we have not made any changes in response to this comment.

Reviewer: *It would also be good to include some of the pressure profiles so that others in the community can check.*

Our Response: Pressure profiles are available in the data files that will be posted on the Combustion Diagnostics Laboratory website and on FigShare, with URLs given in the manuscript. We have endeavored to provide the community with all of the information necessary to reproduce these experiments, including the pressure traces and versions of software packages used in the processing. Moreover, we include several pressure traces with discussion in Section 4.2 of the manuscript. As such, no changes have been made to the manuscript in response to this comment.

Reviewer #3:

Reviewer: *The authors perform a shock tube study measuring ignition delay times of methyl pentanoate, and compare with a kinetic model taken from the literature and one they generated using a Reaction Mechanism Generator, showing that neither model can predict the ignition data satisfactorily; they investigate and discuss possible reasons, but (very reasonably) leave solving this discrepancy as an open challenge to the combustion modeling community.*

Our Response: Thank you for your comments. Detailed responses to each comment are presented below.

Reviewer: *I would suggest using the preferred IUPAC name "Methyl pentanoate" in the title (and mentioning the common name "Methyl valerate" in the abstract and a keyword).*

Our Response: We have modified the title to read "Experiments and Modeling of the Autoignition of Methyl Pentanoate at Low to Intermediate Temperatures and Elevated Pressures in a Rapid Compression Machine", as the reviewer suggests. Methyl valerate and methyl pentanoate are already keywords. We have opted to retain methyl valerate as the primary name used for the compound throughout the text because of the convenient MV acronym (MP is ambiguous, because it could mean methyl propanoate as well).

Reviewer: *Regarding: > "available on the web at <https://combdialab.engr.uconn.edu/database/rcm-database> and on figshare at <https://doi.org/10.6084/m9.figshare.5213341>. In addition, ChemKED-format [33] files are available in the main ChemKED database repository at <https://github.com/pr-omethe-us/ChemKED-database>."*

None of the links work or contain the relevant data. Presumably the authors embargoed it and plan to post it upon acceptance of the manuscript.

But I am pleased to see this sharing of data, as well as the extensive supplementary materials aiding in reproducible science. Bravo.

Our Response: This is indeed the case, and the relevant files will be posted after acceptance. We have double checked that the URLs are correct, just in case. Thank you for your kind words.

Reviewer: *Regarding: > "At 15 bar, the experimental ignition delays are under-predicted by the Diévar et al. [15] model for the three equivalence ratios shown. For the $\phi = 0.25$ and 0.5 conditions, the model appears to be predicting an NTC region of the ignition delays as the temperature decreases"*

Figure 5 does not show, to my eye, any NTC behaviour in the simulations, as asserted in this sentence. Perhaps if the simulations were plotted at a wider range of temperatures (they're simulations, so no experimental reason not to?) this may show up, but at present I feel the figure does not support this statement. For $\phi = 0.5$ simulations are not even plotted over the whole range of the experimental data, let alone extrapolated to lower temperatures where NTC may be predicted.

Our Response: We interpret the increasing curvature of the model response for the $P_C = 15$ bar, $\phi = 0.25$ and 0.5 conditions as the beginning of an NTC region. The RCM simulations are not extrapolated because they use the volume profile associated with a single experiment. However, the simulations are plotted over the whole range of the $\phi = 0.5$ experiments; the large discrepancy between the simulations and experiments causes the illusion that the whole range is not covered.

In addition, we have added a new Fig. 6 that compares adiabatic, constant volume simulations with the model of Diévar et al. [15] with the RCM simulations presented in Fig. 5. The adiabatic, constant volume simulations can be extrapolated over a wide range of temperatures. From Fig. 6, it can be seen that the curvature in the RCM simulations at $P_C = 15$ bar, $\phi = 0.25$ and 0.5 is related to the NTC region of the ignition delay, while the lack of curvature in the $P_C = 15$ bar, $\phi = 2.0$ and the $P_C = 30$ bar, $\phi = 1.0$ simulations is because those lie on the low-temperature side of the predicted NTC.

Reviewer: *I have other questions about possible causes of the discrepancies, but answering them is beyond the reasonable scope of this paper, and the fact that I have them is a good sign regarding the potential impact of this paper. I think people will find it interesting.*

Our Response: Thank you again for your comments. We are also interested in the resolution of these questions, but we agree that they are out of scope for this work.

Experiments and Modeling of the Autoignition of Methyl Pentanoate at Low to Intermediate Temperatures and Elevated Pressures in a Rapid Compression Machine

Bryan W. Weber^{a,*}, Justin A. Bunnell^a, Kamal Kumar^b, Chih-Jen Sung^a

^a*Department of Mechanical Engineering, University of Connecticut, Storrs, CT, USA*

^b*Department of Mechanical Engineering, University of Idaho, Moscow, ID, USA*

Abstract

Methyl valerate ($\text{C}_6\text{H}_{12}\text{O}_2$, methyl pentanoate) is a methyl ester and a relevant surrogate component for biodiesel. In this work, we present ignition delays of methyl valerate measured using a rapid compression machine at a range of engine-relevant temperature, pressure, and equivalence ratio conditions. The conditions we have studied include equivalence ratios (ϕ) from 0.25 to 2.0, temperatures between 680 K and 1050 K, and pressures of 15 bar and 30 bar. The ignition delay data demonstrate a negative temperature coefficient region in the temperature range of 720 K–800 K for both $\phi = 2.0$, 15 bar and $\phi = 1.0$, 30 bar, with two-stage ignition apparent over the narrower temperature ranges of 720 K–760 K for 15 bar and 740 K–760 K at 30 bar. In addition, the experimental ignition delay data are compared with simulations using an existing chemical kinetic model from the literature. The simulations with the literature model under-predict the data by factors between 2 and 10 over the entire range of the experimental data. In addition, a new chemical kinetic model is developed using the Reaction Mechanism Generator (RMG) software. The agreement between the experimental data and the RMG model is also not satisfactory. To help determine the possible reasons for the disagreement, a path analysis of both models is completed. It is found that improvements to both the reaction

*Corresponding Author: bryan.weber@uconn.edu

pathways and thermodynamic properties are required. Further directions for future improvement of the methyl valerate model are discussed.

Keywords: chemical kinetics, rapid compression machine, autoignition, methyl ester, methyl valerate, methyl pentanoate

1. Introduction

For transportation applications, biodiesel is an important constituent in improving environmental friendliness of fuels. This is due to its renewability when produced from sustainable agricultural crops and its ability to reduce emissions relative to petroleum-derived fuels [1]. Biodiesel typically consists of long-chain methyl ester molecules, with typical compositions of C_{14} to C_{20} [1]. Recognizing that the large molecular size of the methyl esters within biodiesel fuel makes creating and using detailed chemical kinetic models challenging [2], it is desired to study their combustion chemistry by studying simpler methyl ester molecules.

A recent review paper summarizes the work on methyl esters relevant to biodiesel combustion [3]; the following summary focuses on ignition delay measurements, since these are the focus of this paper. Autoignition of methyl butanoate (MB, $C_5H_{10}O_2$) has been well-studied in both shock tube and rapid compression machine experiments [4–10]. The prevalence of MB data in the literature is largely due to the early identification of MB as a potential surrogate fuel for biodiesel [11]. However, the literature experiments have shown that MB may not be an appropriate surrogate for biodiesel, due to its lack of negative temperature coefficient (NTC) behavior, a requirement for a suitable biodiesel surrogate [3].

Methyl esters larger than MB, such as methyl valerate (MV, $C_6H_{12}O_2$, methyl pentanoate), have also been studied as possible biodiesel surrogates. Hadj-Ali et al. [9] used a rapid compression machine (RCM) to study the autoignition of several methyl esters including MV. Although MV exhibited two-stage ignition in this study, little additional research has been done on its low-

26 temperature chemistry. Korobeinichev et al. [12] studied MV in premixed lam-
 27 inar flames and extended a detailed high temperature chemical kinetic model
 28 to include MV and methyl hexanoate. Dmitriev et al. [13] added MV to n-
 29 heptane/toluene fuel blends to determine the resulting intermediate species in
 30 premixed flames using a flat burner at 1 atm and an equivalence ratio of 1.75.
 31 The addition of MV helped reduce soot forming intermediates including ben-
 32 zene, cyclopentadienyl, acetylene, propargyl, and vinylacetylene [13]. Hayes
 33 and Burgess [14] computationally examined the peroxy radical isomerization
 34 reactions for MV to better understand the low temperature reaction pathways.
 35 Finally, Diévar et al. [15] used diffusion flames in the counterflow configuration
 36 to determine extinction limits for a number of methyl esters, including MV, and
 37 validated a detailed kinetic model with the experimental data.

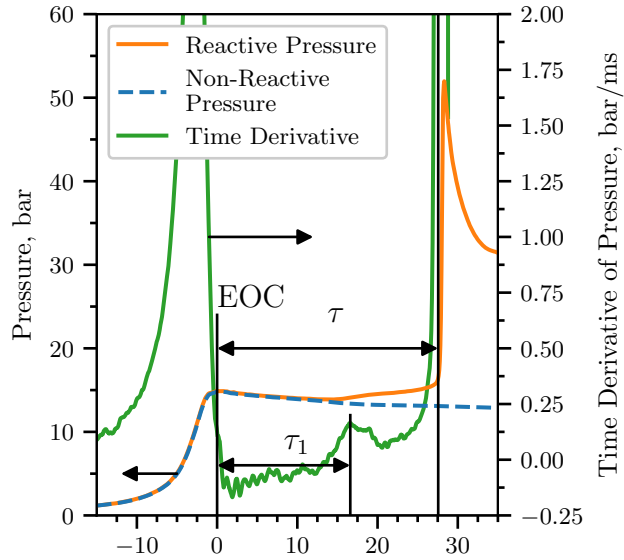
38 This work provides additional data for the autoignition of MV. Data is col-
 39 lected in a RCM under engine relevant conditions spanning from 15 bar to 30 bar,
 40 equivalence ratios (ϕ) from 0.25 to 2.0, and temperatures from 680 K to 1050 K.
 41 The NTC region of MV is mapped out to provide additional information on the
 42 fidelity of using MV as a biodiesel surrogate and insights into the autoignition
 43 chemistry of large methyl esters.

44 **2. Experimental Methods**

45 The RCM used in this study is a single piston arrangement and is pneu-
 46 matically driven and hydraulically stopped. The device has been described in
 47 detail previously [16] and will be described here briefly for reference. The end
 48 of compression (EOC) temperature and pressure (T_C and P_C respectively), are
 49 independently changed by varying the overall compression ratio, initial pressure
 50 (P_0), initial temperature (T_0), and specific heat ratio of the experiments. The
 51 piston in the reaction chamber is machined with a specially designed crevice to
 52 suppress the roll-up vortex effect and promote homogeneous conditions in the
 53 reactor during and after compression [17].

54 The primary diagnostic on the RCM is the in-cylinder pressure measured by

55 a Kistler 6125C dynamic transducer that is compensated for thermal shock. The
 56 transducer is coupled to a Kistler 5010B charge amplifier. The voltage output
 57 of the charge amplifier is recorded by a National Instruments 9125 analog input
 58 device connected to a cDAQ 9178 chassis. The voltage is sampled at a rate of
 59 either 50 kHz or 100 kHz by a LabView VI and processed by a Python package
 60 called UConnRCMPy [18]. Version 3.0.5 of UConnRCMPy [19], 3.6 of Python,
 61 2.3.0 of Cantera [20], 1.13.0 of NumPy [21], 0.19.0 of SciPy [22], and 2.0.1 of
 62 Matplotlib [23] are used in the analysis in this paper.



63

Figure 1: Definition of the ignition delays used in this work. The experiment in this figure
 is conducted for a $\phi = 2.0$ mixture with $\text{Ar}/(\text{N}_2 + \text{Ar}) = 0.5$, $P_0 = 0.7806$ bar, $T_0 = 373$ K,
 $P_C = 14.92$ bar, $T_C = 720$ K, $\tau = (27.56 \pm 0.89)$ ms, and $\tau_1 = (16.60 \pm 0.46)$ ms. The non-
 64 reacting pressure trace by replacing O_2 with N_2 is also shown for reference.

65 The compression stroke of the RCM brings the fuel/oxidizer mixture to the
 66 EOC conditions, and for suitable thermodynamic states, the mixture will ignite
 67 after a delay period. The definitions of the ignition delays are shown in Fig. 1.
 68 The time of the EOC is defined as the maximum of the pressure trace prior to
 69 the start of ignition and the ignition delays are defined as the time from the EOC

until local maxima in the first time derivative of the pressure. Each experimental condition is repeated at least five times to ensure repeatability of the data. As there is some random scatter present in the data, the standard deviation (σ) of the ignition delays from the runs at a given condition is computed. Typically, σ is less than 10 % of the mean values of the overall ignition delay (τ) and the first stage ignition delay (τ_1).

In addition to the reactive experiments, non-reactive experiments are conducted by replacing O_2 with N_2 to determine the influence of machine-specific behavior on the experimental conditions (see Fig. 1) and permit the calculation of the EOC temperature via the isentropic relations between pressure and temperature [24]. The EOC temperature is calculated by the procedure described in Section 3.

The mixtures considered in this study are shown in Table 1. Four equivalence ratios of MV in “air” are considered. While O_2 is kept at 21 % by mole in the oxidizer, the ratio of Ar : N_2 in the oxidizer is varied to adjust the temperatures reached at the EOC. Two P_C conditions are studied in this work, 15 bar and 30 bar, representing engine-relevant conditions. For the $\phi = 2.0$ condition, only $P_C = 15$ bar is considered because we could not achieve T_C values low enough that the ignition during the compression stroke can be prevented.

Table 1: Mixtures considered in this work

| ϕ | Mole Fraction (purity) | | | | Ar/($N_2 + Ar$) |
|--------|------------------------|------------------|---------------|------------------|-------------------|
| | MV (100 %) | O_2 (99.994 %) | Ar (99.999 %) | N_2 (99.999 %) | |
| 0.25 | 0.0065 | 0.2087 | 0.7848 | 0.0000 | 1.0 |
| 0.5 | 0.0130 | 0.2074 | 0.7796 | 0.0000 | 1.0 |
| 1.0 | 0.0256 | 0.2047 | 0.7697 | 0.0000 | 1.0 |
| 1.0 | 0.0256 | 0.2047 | 0.3849 | 0.3848 | 0.5 |
| 2.0 | 0.0499 | 0.1996 | 0.0000 | 0.7505 | 0.0 |
| 2.0 | 0.0499 | 0.1996 | 0.3752 | 0.3753 | 0.5 |

Mixtures are prepared in stainless steel mixing tanks, 17 L and 15 L in size. The proportions of reactants in the mixture are determined by specifying the absolute mass of the fuel, the equivalence ratio, and the ratio of Ar : N₂ in the oxidizer. Mixtures are made by first vacuuming the mixing tanks to an ultimate pressure less than 5 Torr. Since MV is a liquid with a relatively small vapor pressure at room temperature and pressure, it is measured gravimetrically to within 0.01 g of the specified value. The fuel is injected into the mixing tank through a septum. Proportions of O₂, Ar, and N₂ are added manometrically at room temperature and the total pressure is measured by an Omega Engineering MMA100V10T2D0T4A6 type static pressure transducer. The same transducer is used to measure the pressure of the reactant mixture prior to an experiment.

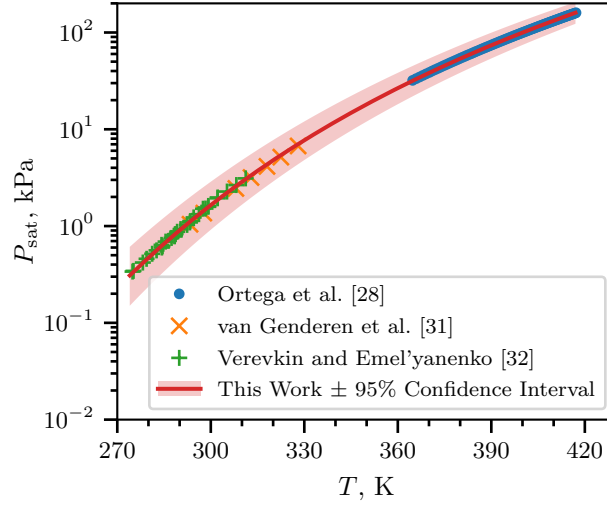
The RCM is equipped with heaters to control the initial temperature of the mixture. After filling in the components to the mixing tanks, the heaters are switched on and the system is allowed 1.5 h to come to steady state. The mixing tanks are also equipped with magnetic stir bars so the reactants are well mixed for the duration of the experiments. Previous work has shown this procedure to completely vaporize the fuel and prevent fuel cracking during the heating process [25–27].

The initial temperature is chosen such that the saturated vapor pressure (P_{sat}) of the fuel at the initial temperature is at least twice the partial pressure of the fuel in the mixing tank. The Antoine equation

$$\log_{10} P_{\text{sat}} = A - \frac{B}{T - C} \quad (1)$$

is used to model the saturated vapor pressure of MV as a function of temperature (T), where A , B , and C are substance-specific coefficients, given in units of K and kPa. Coefficients for Eq. (1) are given in the literature by Ortega et al. [28], Camacho et al. [29], and Stephenson et al. [30]. Unfortunately, the values of the coefficients are different among all three references. Therefore, coefficients for use in Eq. (1) are determined in this work by least squares fitting of the data of Ortega et al. [28], van Genderen et al. [31], and Verevkin and Emel’yanenko [32] using the `curve_fit()` function of SciPy [22] version 0.19.0. Figure 2

119 shows that the coefficients fitted with this procedure give good agreement with
 120 the experimental data; values for the coefficients computed in this work and
 121 reported in the literature works are given in Table 2. The data and code used
 122 to calculate the coefficients are provided in the Supplementary Material.



123

Figure 2: Saturated vapor pressure of MV as a function of temperature, plotted using the
 124 Antoine equation, Eq. (1), with $A = 6.4030$, $B = 1528.69$, and $C = 52.881$.

Table 2: Antoine Equation coefficients computed in this work and obtained from the literature,
 in units of K and kPa. The 2σ confidence interval is estimated by taking the square root of
 125 the diagonals of the covariance matrix returned from `curve_fit()`

| | A | B | C | T_{\min} , K | T_{\max} , K |
|-------------------------------|---------|---------|--------|----------------|----------------|
| This Work | 6.4030 | 1528.69 | 52.881 | 274.9 | 417.18 |
| 2σ Confidence Interval | 0.0919 | 53.47 | 4.934 | — | — |
| 126 Ortega et al. [28] | 6.23175 | 1429.00 | 62.30 | 364.75 | 417.18 |
| Camacho et al. [29] | 5.9644 | 1281.06 | 75.94 | 281 | 547 |
| Stephenson et al. [30] | 6.62646 | 1658.4 | 42.09 | 297 | 411 |

127 3. Computational Methods

128 3.1. RCM Modeling

129 The Python 3.6 interface of Cantera [20] version 2.3.0 is used for all sim-
130 ulations in this work. Detailed descriptions of the use of Cantera for these
131 simulations can be found in the work of Weber and Sung [18] and Dames
132 et al. [33]; a brief overview is given here. As mentioned in Section 2, non-
133 reactive experiments are conducted to characterize the machine-specific effects
134 on the experimental conditions in the RCM. This pressure trace is combined
135 with the reactive pressure trace and used to compute a volume trace by as-
136 suming that the reactants undergo a reversible, adiabatic, constant composition
137 (i.e., isentropic) compression during the compression stroke and an isentropic
138 expansion after the EOC. The volume trace is applied to a simulation con-
139 ducted in an `IdealGasReactor` in Cantera [20] using the CVODES solver from
140 the SUNDIALS suite [34]. The ignition delays from the simulations are de-
141 fined in the same manner as in the experiments. The time derivative of the
142 pressure in the simulation is computed by second order Lagrange polynomials,
143 as discussed by Chapra and Canale [35]. The volume trace files, the corre-
144 sponding pressure traces, and `volume-trace.yaml` files suitable for use with
145 UConnRCMPy v3.0.5 [19] are available on the web at [https://combdialab.](https://combdialab.engr.uconn.edu/database/rcm-database)
146 [engr.uconn.edu/database/rcm-database](https://combdialab.engr.uconn.edu/database/rcm-database) and on figshare at [https://doi.](https://doi.org/10.6084/m9.figshare.5213341)
147 [org/10.6084/m9.figshare.5213341](https://doi.org/10.6084/m9.figshare.5213341). In addition, ChemKED-format [36] files
148 are available in the main ChemKED database repository at [https://github.](https://github.com/pr-ometh-us/ChemKED-database)
149 [com/pr-ometh-us/ChemKED-database](https://github.com/pr-ometh-us/ChemKED-database).

150 To the best of our knowledge, there are three mechanisms for MV combus-
151 tion available in the literature. The first two, by Korobeinichev et al. [12] and
152 Dmitriev et al. [13], were developed to simulate flames, and do not include the
153 low-temperature chemistry necessary to simulate the conditions in the current
154 RCM experiments. The third model was developed by Diévar et al. [15] and
155 includes low-temperature chemistry of MV, although it was only validated by
156 comparison with flame extinction limits. In converting this mechanism for use in

Cantera, we found that there were many species in the thermodynamic database with multiple data entries. For most of these species the thermodynamic data is identical. However, some species are not exact duplicates. For these species, it is not clear from the thermodynamic database file which data set should be preferred. Since Cantera (and CHEMKIN) choose the first instance of a duplicate species to be used, we retained the first entry for all duplicated species. The detailed model of Diévar et al. [15] includes 1105 species and 7141 reactions, and the Cantera formatted input file is available in the Supplementary Material.

3.2. Reaction Mechanism Generator

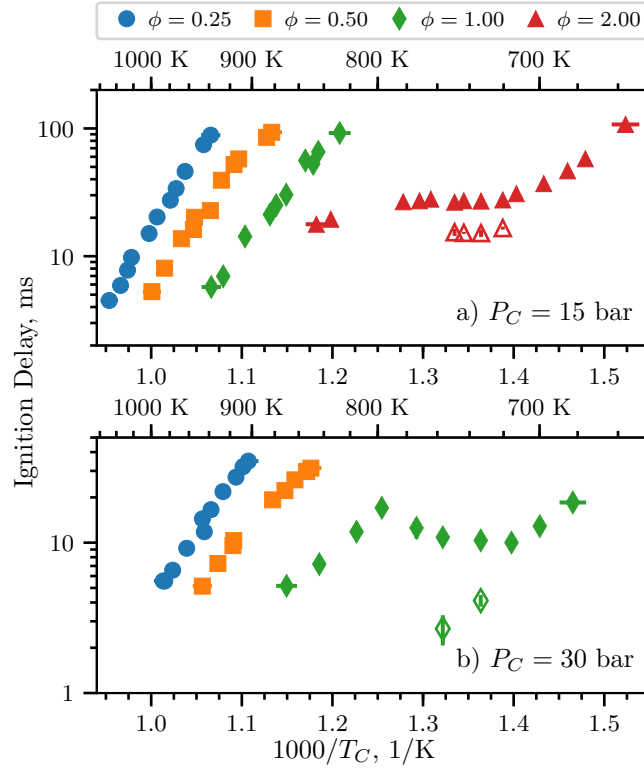
In addition to using a mechanism from the literature, we investigate the use of an automatic mechanism generator, the open-source Reaction Mechanism Generator (RMG) [37] version 2.1.0. The Python version of RMG is used, which requires Python 2.7, and version 2.1.0 of the RMG database is used. The final RMG model contains 427 species and 13640 reactions. Note that the number of species is much lower than the Diévar et al. [15] model because the RMG model focuses on only one fuel (MV), but the number of reactions is substantially higher. The input file used to generate the model is available in the Supplementary Material. In addition, the CHEMKIN and Cantera formatted input files for the RMG-generated model are available in the Supplementary Material.

4. Experimental Results

4.1. Ignition Delays

Figure 3 shows the ignition delay results measured in this study. Filled markers denote the overall ignition delay and hollow markers indicate the first-stage ignition delay. Vertical error bars are drawn on the symbols to represent the 2σ uncertainty in the ignition delay; for many of the experiments, the uncertainty is approximately the same size as the data point, so the error bar is hidden. Horizontal error bars are shown on the first and last points of each equivalence

ratio indicating the estimated uncertainty in the EOC temperature of $\pm 1\%$ [38].
 Fig. 3a shows the results for a compressed pressure of 15 bar, while Fig. 3b shows
 the results for a compressed pressure of 30 bar. Note that $\phi = 2.0$ results were
 not collected for 30 bar, so there are no red triangle data points in Fig. 3b. A
 summary of the ignition delay data is available as a comma-separated value
 file in the Supplementary Material, including the mixture conditions for each
 experiment, the initial conditions, the compressed conditions, and the ignition
 delays and their associated errors.



193

Figure 3: Ignition delays of MV as a function of inverse temperature for varying equivalence ratios. Filled points are the overall ignition delays and hollow points are the first stage ignition delays. a) 15 bar, b) 30 bar.

194

It can be seen from Fig. 3 that the ignition delays for the $\phi = 0.25$ and 0.5 mixtures do not show an NTC region of the ignition delay for both of the pressures studied in this work. However, the $\phi = 1.0$ mixture shows an NTC

198 region at $P_C = 30$ bar between approximately 720 K and 800 K, with measured
 199 first-stage ignition delays at 733 K and 757 K. In addition, the $\phi = 2.0$ mixture
 200 shows an NTC region of ignition delay at 15 bar from approximately 720 K to
 201 780 K, with measured first-stage ignition delays between 720 K and 750 K.

202 Hady-Ali et al. [9] also observed two-stage ignition of MV in stoichiometric
 203 mixtures, stating that “[m]ethyl pentanoate... was more reactive [than methyl
 204 butanoate] with a limit below which autoignition no longer occurs observed at
 205 $T_c = 670$ K and $P_c = 11.4$ bar. At this temperature, the autoignition occurred
 206 in two stages with a clearly identified cool flame event.” However, we do not
 207 find two-stage ignition for the similar pressure of $P_C = 15$ bar in this study.
 208 We note that the stated temperature of the experiment from the work of Hady-
 209 Ali et al. [9] (670 K) is much lower than the lowest temperature we considered
 210 in this work at 15 bar, $\phi = 1.0$ (828 K). We did not conduct experiments at
 211 lower temperatures because the work of Mittal and Sung [17] showed that the
 212 temperature field in the RCM reaction chamber was uniform for approximately
 213 100 ms after the EOC, and our measured ignition delay at 15 bar, $\phi = 1.0$, and
 214 828 K is 92.14 ms.

215 However, we find NTC behavior of the overall ignition delay and two-stage
 216 ignition at the higher pressure of 30 bar, and at higher temperatures than those
 217 reported for two-stage ignition in the study of Hady-Ali et al. [9]. The trend
 218 of NTC behavior shifting to higher temperatures with increasing pressure can
 219 be seen in other classes of fuels. Kukkadapu et al. [39] found a similar trend
 220 in gasoline composed of iso-alkanes, n-alkanes, cyclo-alkanes, aromatics, and
 221 olefins. Kukkadapu et al. [39] attributed the shift of the NTC region to the
 222 reactions between the hydroperoxyalkyl radical (QOOH) and O_2 becoming more
 223 dominant than the unimolecular decomposition of QOOH at higher pressures.
 224 Similar trends could occur for the hydroperoxyalkyl radicals of MV.

225 To further understand the effect of the methyl ester functional group on the
 226 NTC region of ignition delay, we compare with the alkane and alcohol with
 227 5-carbon alkyl chains, n-pentane and n-pentanol. n-Pentane and MV have the
 228 same fuel mole percentage for stoichiometric mixtures in air (2.56 %), while

229 n-pentanol has a fuel mole percentage of 2.72 % for stoichiometric conditions.
 230 Ribaucour et al. [40] and Bugler et al. [41] found the NTC region for n-pentane
 231 to be between 760 K and 910 K at pressures near 10 atm. As we will compare
 232 with our MV data at 30 bar, we note that increasing the pressure tends to shift
 233 the NTC to higher temperatures, as mentioned previously [39]. Heufer et al. [42]
 234 found NTC behavior for n-pentanol in the range of 770 K to 900 K at 30 bar. In
 235 this study, we find the NTC window for MV at 30 bar to be between 720 K and
 236 800 K. Therefore, it appears that the methyl ester functional group causes the
 237 NTC range to occur at lower temperature as compared to alkanes and alcohols
 238 with similar alkyl chain lengths. This result was also noted by Hadj-Ali et al.
 239 [9] for methyl hexanoate as the fuel.

240 4.2. Pressure Traces

241 Figure 4a shows the pressure traces for selected experiments at $\phi = 1.0$, $P_C =$
 242 30 bar. The three reactive pressure traces shown are at the low-temperature end
 243 of the NTC (blue, 700 K), one case with two-stage ignition (orange, 733 K), and
 244 one case near the high-temperature limit of the NTC region (green, 774 K). Also
 245 shown is the non-reactive pressure trace for the 700 K case (red). By comparing
 246 the 700 K pressure trace with the non-reactive pressure trace, it can be seen
 247 that there is substantial heat release prior to main ignition as measured by the
 248 deviation of the reactive pressure trace from the non-reactive trace. However,
 249 there is only one peak in the time derivative of the pressure, so no first-stage
 250 ignition delay is defined for this case. It can also be seen in Fig. 4a that the
 251 774 K case shows some heat release prior to ignition, although again there is
 252 only one peak in the time derivative of the pressure. Furthermore, the heat
 253 release at 774 K appears to be more gradual than at 700 K.

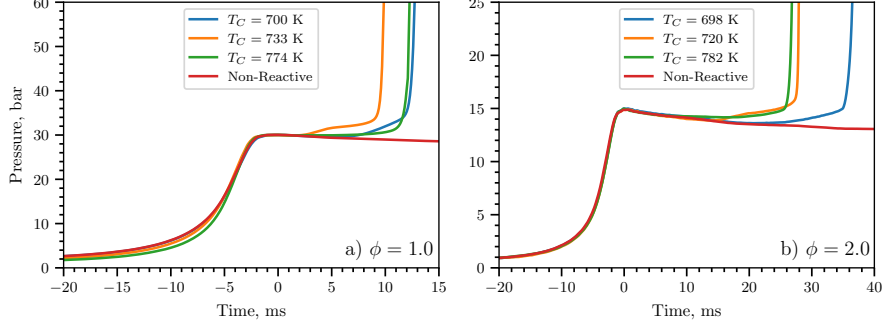


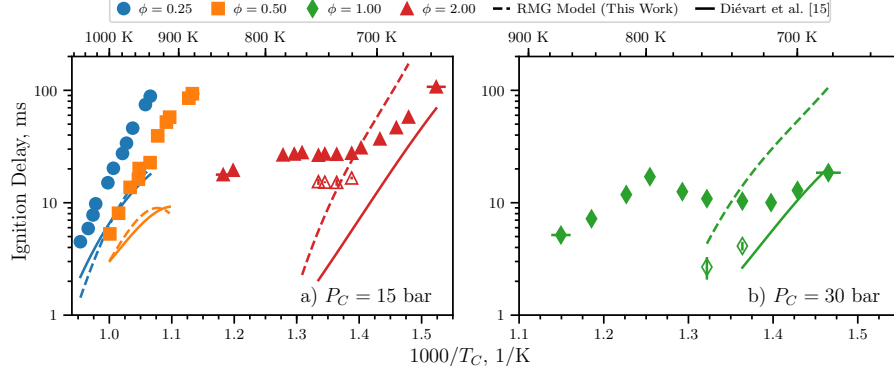
Figure 4: Selected pressure traces around the NTC region of ignition delay. a) $\phi = 1.0$, $P_C = 30$ bar, b) $\phi = 2.0$, $P_C = 15$ bar. The corresponding non-reactive pressure traces are also included for reference.

A similar trend can be observed in Fig. 4b for $\phi = 2.0$ at $P_C = 15$ bar, where pressure traces at several points around the NTC region are plotted. As in Fig. 4a, the three reactive pressure traces shown are at the low-temperature end of the NTC (blue, 698 K), one case with two-stage ignition (orange, 720 K), and one case near the high-temperature limit of the NTC region (green, 782 K). Also shown is the non-reactive pressure trace for the 698 K case (red). As for the $\phi = 1.0$ case, the pressure traces show significant heat release prior to the overall ignition, as judged by deviation from the non-reactive case.

5. Computational Results

Figure 5 compares experimentally measured overall ignition delays with ignition delays computed with the detailed model of Diévar et al. [15] (solid lines). Figure 5a shows results at $P_C = 15$ bar, while Fig. 5b shows results at $P_C = 30$ bar. Only some equivalence ratios are shown for each pressure condition; data and simulated results are not shown for cases where the reactive simulated temperature at the EOC deviated substantially from the non-reactive temperature due to heat release during the compression stroke. Furthermore, it is important to note that the model of Diévar et al. [15] was not validated for MV ignition delays, only for extinction strain rates.

274



275

Figure 5: Comparison of experimental (τ and τ_1) and simulated (τ) ignition delays computed using the procedure described in Section 3.1. a) 15 bar, b) 30 bar.

At 15 bar, the experimental overall ignition delays are under-predicted by the Diévert et al. [15] model for the three equivalence ratios shown. For the $\phi = 0.25$ and 0.5 conditions, the model appears to be predicting an NTC region of the overall ignition delays as the temperature decreases, as judged by the increasing curvature of the simulations, although such a trend is not observed for the experimental data. However, at $\phi = 2.0$, the model does not predict the presence of an NTC region, although one is present in the experiments. Nonetheless, the agreement seems to be improving as the temperature is decreased. Comparing the Diévert et al. [15] model to the stoichiometric data at 30 bar, we find a similar trend as the $\phi = 2.0$, $P_C = 15$ bar data. The model does not predict the NTC region found experimentally for the $\phi = 1.0$, $P_C = 30$ bar experiments, but the agreement improves as the temperature decreases. Interestingly, two-stage ignition is predicted for all of the $\phi = 1.0$ and $\phi = 2.0$ data shown in Fig. 5. However, the first-stage ignition delays are 0.1 ms to 0.5 ms less than the overall ignition delays, and are not shown on Fig. 5 because they are nearly indistinguishable from the overall ignition delay.

To further understand the model of Diévert et al. [15], we have conducted adiabatic, constant volume simulations (called CONV simulations), as these simulations are not linked to a particular experiment by the volume trace and

296 can be conducted over a wide range of temperatures. In the CONV simulations,
 297 overall ignition delay is defined as an increase in the temperature of 400 K over
 298 the initial temperature. The diluent for all of the CONV simulations is pure
 299 argon, although the RCM simulations described previously consider the diluent
 300 mixture associated with each experiment (either pure argon or a 50:50 mixture
 301 of argon and nitrogen by mole, see Table 1 and the Supplementary Material).

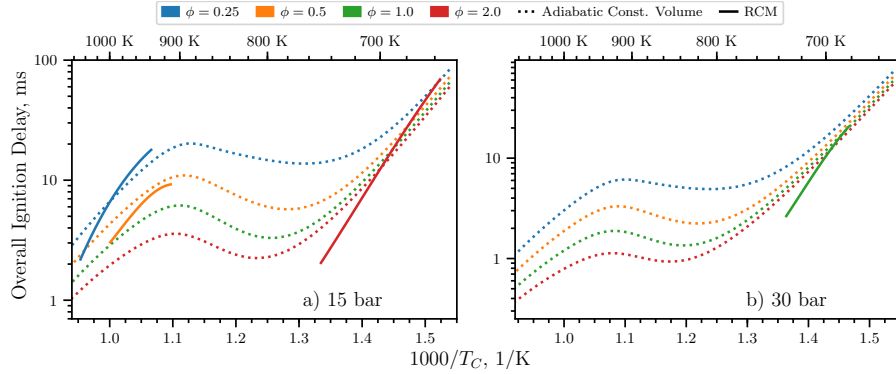


Figure 6: Comparison of simulated overall ignition delays computed in an adiabatic, constant volume system (dotted lines) and computed using the procedure described in Section 3.1 (solid lines). a) 15 bar, b) 30 bar.

304 Figure 6 compares the CONV simulations to the RCM simulations shown in
 305 Fig. 5. From Fig. 6, it can be seen that the curvature in the RCM simulations
 306 at $P_C = 15$ bar, $\phi = 0.25$ and 0.5 is related to the NTC region of the overall
 307 ignition delay, while the lack of curvature in the $P_C = 15$ bar, $\phi = 2.0$ and the
 308 $P_C = 30$ bar, $\phi = 1.0$ simulations is because those lie on the low-temperature
 309 side of the predicted NTC. It is clear from Fig. 6 that the model of Diévert
 310 et al. [15] predicts the NTC to occur at too high a temperature relative to the
 311 experiments.

312 To elucidate the underlying reasons for the disagreement between the Diévert
 313 et al. [15] model and the data, we conduct simulations with an additional model
 314 constructed using RMG (see Section 3.2). As can be seen in Fig. 5a, the agree-
 315 ment between the RMG model (dashed lines) and the experimental data is
 316 similar to the Diévert et al. [15] model for the $P_C = 15$ bar, $\phi = 0.25$ and 0.5

317 data. Moreover, the RMG model predicts a similar NTC region as temperature
 318 is decreasing. For the $P_C = 15$ bar, $\phi = 2.0$ data, the RMG model tends to
 319 over-predict the low-temperature overall ignition delays (i.e., those to the right
 320 of the experimental NTC region on the Arrhenius plot), and does not predict the
 321 NTC region found experimentally. As before, the trend at $P_C = 30$ bar, $\phi = 1.0$
 322 is similar to the $P_C = 15$ bar, $\phi = 2.0$ data; the RMG model over-predicts the
 323 low-temperature overall ignition delays and does not predict the experimental
 324 NTC region. Finally, as in the Diévert et al. [15] model, two-stage ignition is
 325 predicted for all of the $\phi = 1.0$ and $\phi = 2.0$ data shown in Fig. 5. However,
 326 the first-stage ignition delays are 0.1 ms to 0.5 ms less than the overall ignition
 327 delays, and are not shown on Fig. 5 because they are nearly indistinguishable
 328 from the overall ignition delay.

329 It is clear that neither model is able to predict the ignition delays of MV
 330 particularly well. In addition to the poor agreement shown in Fig. 5, the simu-
 331 lations for $P_C = 15$ bar, $\phi = 1.0$ and $P_C = 30$ bar, $\phi = 0.25, 0.5$ and 2.0 showed
 332 substantial heat release during the compression stroke (i.e., the simulations are
 333 much too reactive), and so these conditions are not compared in Fig. 5. We note
 334 again that the model by Diévert et al. [15] was validated for MV combustion
 335 only by comparison to flame extinction limits, so the disagreement is not wholly
 336 surprising.

337 In general, there could be three likely sources of error in the models: missing
 338 reaction pathways, incorrect values of the reaction rates, and incorrect values
 339 for thermodynamic properties of the species. We have noted in Section 3.2 that
 340 the RMG model has many more reactions than the Diévert et al. [15] model
 341 and the algorithm used in RMG considers a substantial number of the possible
 342 pathways. This reduces the possibility of missing reaction pathways affecting
 343 the model. Further detailed studies are required to ensure that the RMG model
 344 includes all of the relevant reaction pathways, which are outside the scope of
 345 this work.

346 The second source of error may be incorrect reaction rate parameters, either
 347 because the rates are specified incorrectly in the model or because the rates are

not well estimated by the typical analogy based-rules. It should be noted that errors of this type may affect the model generated by RMG—if the rates are not estimated correctly, reactions that are important in reality may not be included in the model. Determining the accuracy of the reaction rates used in the RMG and Diévar et al. [15] models requires further detailed studies of the models, which are also outside the scope of this work. Another, related, source of error could be incorrect estimation of the pressure dependence of the reaction rates, which may be particularly important for the isomerization reactions prevalent in low-temperature chemistry.

The third source of error may lie in the estimation of the thermodynamic properties of the species, particularly the fuel radicals. In the work of Diévar et al. [15], the program THERM [43] was used to estimate thermodynamic values using the group additivity method. In the RMG model constructed in this work, RMG itself estimates the thermodynamic properties of the molecules also using the group additivity method. Nonetheless, the two models have differing predictions of the thermodynamic properties of the species in the model, particularly the fuel and its radicals. The values of the heats of formation of the fuel and its H-atom abstraction radicals are shown in Table 3; the radicals are labeled according to the convention shown in Fig. 7.

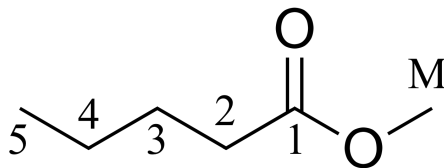


Figure 7: Structure of MV with carbon atoms labeled according to the convention used in Table 3 and Table 4

Table 3 shows that the heats of formation of the fuel and radicals 3, 4, 5, and M are quite similar between the two mechanisms. However, the heat of formation of the second radical, the one closest to the methyl ester group, has a significantly lower heat of formation in the model by Diévar et al. [15] than in the RMG model. Note that it is expected that the second radical will

374 be somewhat more stable than the other radicals, due to the influence of the
 375 methyl ester group on the adjacent carbon atom.

Table 3: Heats of formation of MV and its radicals, labeled according to the convention used
 376 in Fig. 7

| Radical Site | Diévert et al. [15] | | RMG Model (this work) | |
|--------------|---------------------|------------|-----------------------|------------|
| | [kJ/mol] | [kcal/mol] | [kJ/mol] | [kcal/mol] |
| MV | -470.98 | -112.57 | -472.53 | -112.94 |
| 2 | -297.16 | -71.02 | -273.63 | -65.40 |
| 3 | -277.03 | -66.21 | -273.63 | -65.40 |
| 4 | -277.03 | -66.21 | -278.61 | -66.59 |
| 5 | -265.94 | -63.56 | -267.53 | -63.94 |
| M | -270.51 | -64.65 | -270.12 | -64.56 |

378 This difference in heats of formation affects the pathways that consume the
 379 fuel. By conducting a reaction pathway analysis to determine which radicals are
 380 formed from the breakdown of the fuel, we can analyze the proportion of each
 381 radical formed as the fuel breaks down during the autoignition process. The
 382 following analysis is conducted for a constant volume, adiabatic simulation with
 383 initial temperature and pressure of 700 K and 30 bar, respectively, and for the
 384 stoichiometric equivalence ratio. The rates of production of the species have
 385 been integrated until the time of 20 % fuel consumption. The results of this
 386 analysis are shown in Table 4 for the two models. The percentages shown in
 387 Table 4 are the percent of the fuel consumed to form a particular fuel radical
 388 by all the reactions that can form that radical, and the radicals are labeled
 389 according to the convention in Fig. 7.

390 At the relatively low temperature and high pressure condition of this analy-
 391 sis, all of the fuel is consumed by H-atom abstractions to form the fuel radicals
 392 shown. It can be seen that the two models have quite different distributions
 393 of products from the first H-abstraction reactions. The model of Diévert et al.
 394 [15] predicts that H-abstraction from the second carbon is the most prevalent,

while the RMG model predicts that the radical on the fourth carbon in the chain will be primarily formed. This is in line with the heats of formation in Table 3, where the most stable radical (i.e., the radical with the smallest heat of formation) is most likely to be formed in each model.

Table 4: Percent of MV consumed to form fuel radical species with a hydrogen atom missing at the location indicated in the first column and Fig. 7

| Radical Site | Diévert et al. [15] [%] | RMG Model [%] | RMG switched [%] |
|--------------|-------------------------|---------------|------------------|
| 2 | 29.2 | 12.5 | 11.0 |
| 3 | 17.5 | 12.2 | 11.1 |
| 4 | 17.5 | 50.6 | 56.6 |
| 5 | 9.5 | 3.9 | 4.3 |
| M | 26.3 | 20.8 | 16.9 |

To further compare the models with each other, the NASA polynomials representing the thermodynamic properties of MV and the 5 fuel radicals from the model of Diévert et al. [15] are used to replace the equivalent molecules in the RMG model. The results of a path analysis at the same condition as the other analysis is shown in Table 4 in the “RMG switched” column. The results of the analysis of the “RMG switched” model show that the radical on the fourth carbon is still the most prevalent, despite the heats of formation for the fuel radicals in the “RMG switched” model being identical to the Diévert et al. [15] model. This suggests that the reaction pathways have a substantial impact on the simulation, in addition to the influence of the thermochemistry, as discussed previously. Moreover, since the thermochemistry of the species in a reaction controls the reverse reaction rate of a reaction, the RMG algorithm may miss important pathways due to improperly estimated thermochemistry.

Taken together, these results show that the poor performance in a given model cannot be attributed to a single source. Separating the influence of thermochemistry and kinetics requires further detailed study of the methyl valerate system specifically, and methyl ester systems more generally. Although such

419 detailed work has begun, for example, with the work of Hayes and Burgess
420 [14], further work is required to accurately predict the low temperature ignition
421 delays of methyl valerate.

422 6. Conclusions

423 In this study, we have measured ignition delays for methyl valerate over a
424 wide range of engine-relevant pressures, temperatures, and equivalence ratios.
425 An NTC region of the overall ignition delay and two-stage ignition are recorded
426 for pressures of 15 bar at $\phi = 2.0$ and 30 bar at $\phi = 1.0$. A detailed chemical
427 kinetic model available in the literature is unable to reproduce the experimental
428 results, so a new model is constructed using the Reaction Mechanism Generator
429 software. Although the new model contains many more reactions than the
430 literature model, it is still unable to predict the experimental ignition delays
431 satisfactorily. Both models predict an NTC region of the overall ignition delay
432 under conditions where none is found in the experiments, and fail to predict
433 the NTC region of overall ignition delay that is present in the experiments.
434 Possible reasons for the discrepancy include missing reaction pathways, incorrect
435 rate estimates, and incorrect thermodynamic property estimates. Comparative
436 analysis of the two models failed to identify a single source of the error, and
437 further detailed studies are required to improve predictions of the ignition delay
438 at these engine-relevant conditions.

439 7. Acknowledgments

440 The authors acknowledge support from the Combustion Energy Frontier
441 Research Center, an Energy Frontier Research Center funded by the U.S. De-
442 partment of Energy, Office of Science, Office of Basic Energy Sciences, under
443 award number DE-SC0001198.

References

- [1] S. K. Hoekman, C. Robbins. Review of the effects of biodiesel on NO_x emissions. *Fuel Processing Technology* 96 (2012) 237–249. doi:10.1016/j.fuproc.2011.12.036.
- [2] J. Y. Lai, K. C. Lin, A. Violi. Biodiesel combustion: Advances in chemical kinetic modeling. *Progress in Energy and Combustion Science* 37 (2011) 1–14. doi:10.1016/j.pecs.2010.03.001.
- [3] L. Coniglio, H. Bennadji, P. Glaude, O. Herbinet, F. Billaud. Combustion chemical kinetics of biodiesel and related compounds (methyl and ethyl esters): Experiments and modeling – Advances and future refinements. *Progress in Energy and Combustion Science* 39 (2013) 340–382. doi:10.1016/j.pecs.2013.03.002.
- [4] W. K. Metcalfe, S. Dooley, H. J. Curran, J. M. Simmie, A. M. El-Nahas, M. V. Navarro. Experimental and modeling study of C₅H₁₀O₂ ethyl and methyl esters. *The Journal of Physical Chemistry A* 111 (2007) 4001–4014. doi:10.1021/jp067582c.
- [5] S. M. Walton, M. S. Wooldridge, C. K. Westbrook. An experimental investigation of structural effects on the auto-ignition properties of two C₅ esters. *Proceedings of the Combustion Institute* 32 (2009) 255–262. doi:10.1016/j.proci.2008.06.208.
- [6] S. Dooley, H. J. Curran, J. M. Simmie. Autoignition measurements and a validated kinetic model for the biodiesel surrogate, methyl butanoate. *Combustion and Flame* 153 (2008) 2–32. doi:10.1016/j.combustflame.2008.01.005.
- [7] B. Akih-Kumgeh, J. M. Bergthorson. Comparative Study of Methyl Butanoate and n -Heptane High Temperature Autoignition. *Energy & Fuels* 24 (2010) 2439–2448. doi:10.1021/ef901489k.

- 471 [8] B. Akih-Kumgeh, J. M. Bergthorson. Structure-reactivity trends of C1–C4
472 alkanoic acid methyl esters. *Combustion and Flame* 158 (2011) 1037–1048.
473 doi:10.1016/j.combustflame.2010.10.021.
- 474 [9] K. Hadj-Ali, M. Crochet, G. Vanhove, M. Ribaucour, R. Minetti. A study
475 of the low temperature autoignition of methyl esters. *Proceedings of the*
476 *Combustion Institute* 32 (2009) 239–246. doi:10.1016/j.proci.2008.09.002.
- 477 [10] K. Kumar, C.-J. Sung. Autoignition of methyl butanoate under en-
478 gine relevant conditions. *Combustion and Flame* 171 (2016) 1–14.
479 doi:10.1016/j.combustflame.2016.04.011.
- 480 [11] E. Fisher, W. J. Pitz, H. J. Curran, C. K. Westbrook. Detailed chem-
481 ical kinetic mechanisms for combustion of oxygenated fuels. *Proceed-*
482 *ings of the Combustion Institute* 28 (2000) 1579–1586. doi:10.1016/S0082-
483 0784(00)80555-X.
- 484 [12] O. Korobeinichev, I. Gerasimov, D. Knyazkov, A. Shmakov, T. Bolshova,
485 N. Hansen, C. K. Westbrook, G. Dayma, B. Yang. An Experimental and
486 Kinetic Modeling Study of Premixed Laminar Flames of Methyl Pentanoate
487 and Methyl Hexanoate. *Zeitschrift für Physikalische Chemie* 229 (2015).
488 doi:10.1515/zpch-2014-0596.
- 489 [13] A. M. Dmitriev, D. A. Knyazkov, T. A. Bolshova, A. G. Shmakov,
490 O. P. Korobeinichev. The effect of methyl pentanoate addition on
491 the structure of premixed fuel-rich n-heptane/toluene flame at at-
492 mospheric pressure. *Combustion and Flame* 162 (2015) 1964–1975.
493 doi:10.1016/j.combustflame.2014.12.015.
- 494 [14] C. Hayes, D. R. Burgess. Exploring the oxidative decompositions of methyl
495 esters: Methyl butanoate and methyl pentanoate as model compounds for
496 biodiesel. *Proceedings of the Combustion Institute* 32 (2009) 263–270.
497 doi:10.1016/j.proci.2008.05.075.

- [15] P. Diévar, S. H. Won, J. Gong, S. Dooley, Y. Ju. A comparative study of the chemical kinetic characteristics of small methyl esters in diffusion flame extinction. *Proceedings of the Combustion Institute* 34 (2013) 821–829. doi:10.1016/j.proci.2012.06.180.
- [16] G. Mittal, C.-J. Sung. A Rapid Compression Machine for Chemical Kinetics Studies at Elevated Pressures and Temperatures. *Combustion Science and Technology* 179 (2007) 497–530. doi:10.1080/00102200600671898.
- [17] G. Mittal, C.-J. Sung. Aerodynamics inside a rapid compression machine. *Combustion and Flame* 145 (2006) 160–180. doi:10.1016/j.combustflame.2005.10.019.
- [18] B. W. Weber, C.-J. Sung. UConnRCMPy: Python-based Data Analysis for Rapid Compression Machines. in: S. Benthall, S. Rostrup (Eds.), *Proceedings of the 15th Python in Science Conference*, pp. 36–44. http://conference.scipy.org/proceedings/scipy2016/bryan_weber.html.
- [19] B. W. Weber, R. Fang, C.-J. Sung. UConnRCMPy, 2017. v3.0.5. doi:10.5281/zenodo.815569.
- [20] D. G. Goodwin, H. K. Moffat, R. L. Speth. Cantera: An Object-oriented Software Toolkit for Chemical Kinetics, Thermodynamics, and Transport Processes, 2017. v2.3.0. doi:10.5281/zenodo.170284.
- [21] S. van der Walt, S. C. Colbert, G. Varoquaux. The NumPy Array: A Structure for Efficient Numerical Computation. *Computing in Science & Engineering* 13 (2011) 22–30. doi:10.1109/MCSE.2011.37.
- [22] E. Jones, T. Oliphant, P. Peterson, et al. SciPy: Open source scientific tools for Python, 2001–. <https://scipy.org>.
- [23] J. D. Hunter. Matplotlib: A 2D Graphics Environment. *Computing in Science & Engineering* 9 (2007) 90–95. doi:10.1109/MCSE.2007.55.

- [24] D. Lee, S. Hochgreb. Rapid Compression Machines: Heat Transfer and Suppression of Corner Vortex. *Combustion and Flame* 114 (1998) 531–545. doi:10.1016/S0010-2180(97)00327-1.
- [25] B. W. Weber, K. Kumar, Y. Zhang, C.-J. Sung. Autoignition of n-butanol at elevated pressure and low-to-intermediate temperature 158 (???) 809–819. doi:10.1016/j.combustflame.2011.02.005.
- [26] K. Kumar, G. Mittal, C.-J. Sung. Autoignition of n-decane under elevated pressure and low-to-intermediate temperature conditions 156 (???) 1278–1288. doi:10.1016/j.combustflame.2009.01.009.
- [27] A. K. Das, C.-J. Sung, Y. Zhang, G. Mittal. Ignition delay study of moist hydrogen/oxidizer mixtures using a rapid compression machine 37 (???) 6901–6911. doi:10.1016/j.ijhydene.2012.01.111.
- [28] J. Ortega, F. Espiau, J. Tojo, J. Canosa, A. Rodríguez. Isobaric Vapor-Liquid Equilibria and Excess Properties for the Binary Systems of Methyl Esters + Heptane. *Journal of Chemical & Engineering Data* 48 (2003) 1183–1190. doi:10.1021/je030117d.
- [29] A. G. Camacho, J. M. Moll, S. Canzonieri, M. A. Postigo. Vapor-Liquid Equilibrium Data for the Binary Methyl Esters (Butyrate, Pentanoate, and Hexanoate) (1) + Propanenitrile (2) Systems at 93.32 kPa. *Journal of Chemical & Engineering Data* 52 (2007) 871–875. doi:10.1021/je060469v.
- [30] R. M. Stephenson, S. Malanowski, D. Ambrose, *Handbook of the Thermodynamics of Organic Compounds*, Elsevier, New York, 1987.
- [31] A. C. van Genderen, J. van Miltenburg, J. G. Blok, M. J. van Bommel, P. J. van Ekeren, G. J. van den Berg, H. A. Oonk. Liquid–vapour equilibria of the methyl esters of alkanolic acids: Vapour pressures as a function of temperature and standard thermodynamic function changes. *Fluid Phase Equilibria* 202 (2002) 109–120. doi:10.1016/S0378-3812(02)00097-3.

- 551 [32] S. P. Verevkin, V. N. Emel'yanenko. Transpiration method: Vapor pres-
552 sures and enthalpies of vaporization of some low-boiling esters. *Fluid Phase*
553 *Equilibria* 266 (2008) 64–75. doi:10.1016/j.fluid.2008.02.001.
- 554 [33] E. E. Dames, A. S. Rosen, B. W. Weber, C. W. Gao, C.-J. Sung,
555 W. H. Green. A detailed combined experimental and theoretical study
556 on dimethyl ether/propane blended oxidation. *Combustion and Flame* 168
557 (2016) 310–330. doi:10.1016/j.combustflame.2016.02.021.
- 558 [34] A. C. Hindmarsh, P. N. Brown, K. E. Grant, S. L. Lee, R. Serban, D. E.
559 Shumaker, C. S. Woodward. SUNDIALS: Suite of nonlinear and differen-
560 tial/algebraic equation solvers. *ACM Transactions on Mathematical Soft-*
561 *ware* 31 (2005) 363–396. doi:10.1145/1089014.1089020.
- 562 [35] S. C. Chapra, R. P. Canale, *Numerical Methods for Engineers*, McGraw-
563 Hill Higher Education, Boston, 6th ed edition, 2010.
- 564 [36] B. W. Weber, K. E. Niemeyer. ChemKED: A human- and machine-readable
565 data standard for chemical kinetics experiments. Submitted to: *Interna-*
566 *tional Journal of Chemical Kinetics* (2017). [arXiv:1706.01987](https://arxiv.org/abs/1706.01987).
- 567 [37] J. W. Allen, C. F. Goldsmith, W. H. Green. Automatic estimation of
568 pressure-dependent rate coefficients. *Physical Chemistry Chemical Physics*
569 14 (2012) 1131–1155. doi:10.1039/c1cp22765c.
- 570 [38] B. W. Weber, C.-J. Sung, M. W. Renfro. On the uncertainty of temperature
571 estimation in a rapid compression machine. *Combustion and Flame* 162
572 (2015) 2518–2528. doi:10.1016/j.combustflame.2015.03.001.
- 573 [39] G. Kukkadapu, K. Kumar, C.-J. Sung, M. Mehl, W. J. Pitz. Exper-
574 imental and surrogate modeling study of gasoline ignition in a rapid
575 compression machine. *Combustion and Flame* 159 (2012) 3066–3078.
576 doi:10.1016/j.combustflame.2012.05.008.
- 577 [40] M. Ribaucour, R. Minetti, L. R. Sochet. Autoignition of n-pentane
578 and 1-pentene: Experimental data and kinetic modeling. *Symposium*

- 579 (International) on Combustion 27 (1998) 345–351. doi:10.1016/S0082-
580 0784(98)80422-0.
- 581 [41] J. Bugler, K. P. Somers, E. J. Silke, H. J. Curran. Revisiting the Ki-
582 netics and Thermodynamics of the Low-Temperature Oxidation Pathways
583 of Alkanes: A Case Study of the Three Pentane Isomers. The Journal of
584 Physical Chemistry A 119 (2015) 7510–7527. doi:10.1021/acs.jpca.5b00837.
- 585 [42] K. A. Heufer, J. Bugler, H. J. Curran. A comparison of longer alkane
586 and alcohol ignition including new experimental results for n-pentanol and
587 n-hexanol. Proceedings of the Combustion Institute 34 (2013) 511–518.
588 doi:10.1016/j.proci.2012.05.103.
- 589 [43] E. R. Ritter, J. W. Bozzelli. THERM: Thermodynamic property estimation
590 for gas phase radicals and molecules. International Journal of Chemical
591 Kinetics 23 (1991) 767–778. doi:10.1002/kin.550230903.

Experiments and Modeling of the Autoignition of Methyl ~~Valerate~~ Pentanoate at Low to Intermediate Temperatures and Elevated Pressures in a Rapid Compression Machine

Bryan W. Weber^{a,*}, Justin A. Bunnell^a, Kamal Kumar^b, Chih-Jen Sung^a

^a*Department of Mechanical Engineering, University of Connecticut, Storrs, CT, USA*

^b*Department of Mechanical Engineering, University of Idaho, Moscow, ID, USA*

Abstract

Methyl valerate ($\text{C}_6\text{H}_{12}\text{O}_2$, methyl pentanoate) is a methyl ester and a relevant surrogate component for biodiesel. In this work, we present ignition delays of methyl valerate measured using a rapid compression machine at a range of engine-relevant temperature, pressure, and equivalence ratio conditions. The conditions we have studied include equivalence ratios (ϕ) from 0.25 to 2.0, temperatures between 680 K and 1050 K, and pressures of 15 bar and 30 bar. The ignition delay data demonstrate a negative temperature coefficient region in the temperature range of 720 K–800 K for both $\phi = 2.0$, 15 bar and $\phi = 1.0$, 30 bar, with two-stage ignition apparent over the narrower temperature ranges of 720 K–760 K for 15 bar and 740 K–760 K at 30 bar. In addition, the experimental ignition delay data are compared with simulations using an existing chemical kinetic model from the literature. The simulations with the literature model under-predict the data by factors between 2 and 10 over the entire range of the experimental data. In addition, a new chemical kinetic model is developed using the Reaction Mechanism Generator (RMG) software. The agreement between the experimental data and the RMG model is also not satisfactory. To help determine the possible reasons for the disagreement, a path analysis of both models is completed. It is found that improvements to both the reaction

*Corresponding Author: bryan.weber@uconn.edu

pathways and thermodynamic properties are required. Further directions for future improvement of the methyl valerate model are discussed.

Keywords: chemical kinetics, rapid compression machine, autoignition, methyl ester, methyl valerate, methyl pentanoate

1. Introduction

For transportation applications, biodiesel is an important constituent in improving environmental friendliness of fuels. This is due to its renewability when produced from sustainable agricultural crops and its ability to reduce emissions relative to petroleum-derived fuels [1]. Biodiesel typically consists of long-chain methyl ester molecules, with typical compositions of C_{14} to C_{20} [1]. Recognizing that the large molecular size of the methyl esters within biodiesel fuel makes creating and using detailed chemical kinetic models challenging [2], it is desired to study their combustion chemistry by studying simpler methyl ester molecules.

A recent review paper summarizes the work on methyl esters relevant to biodiesel combustion [3]; the following summary focuses on ignition delay measurements, since these are the focus of this paper. Autoignition of methyl butanoate (MB, $C_5H_{10}O_2$) has been well-studied in both shock tube and rapid compression machine experiments [4–10]. The prevalence of MB data in the literature is largely due to the early identification of MB as a potential surrogate fuel for biodiesel [11]. However, the [literature](#) experiments have shown that MB may not be an appropriate surrogate for biodiesel, due to its lack of negative temperature coefficient (NTC) behavior, a requirement for a suitable biodiesel surrogate [3].

Methyl esters larger than MB, such as methyl valerate (MV, $C_6H_{12}O_2$, methyl pentanoate), have also been studied as possible biodiesel surrogates. Hadj-Ali et al. [9] used a rapid compression machine (RCM) to study the autoignition of several methyl esters including MV. Although MV exhibited two-stage ignition in this study, little additional research has been done on its low-

26 temperature chemistry. Korobeinichev et al. [12] studied MV in premixed lam-
 27 inar flames and extended a detailed high temperature chemical kinetic model
 28 to include MV and methyl hexanoate. Dmitriev et al. [13] added MV to n-
 29 heptane/toluene fuel blends to determine the resulting intermediate species in
 30 premixed flames using a flat burner at 1 atm and an equivalence ratio of 1.75.
 31 The addition of MV helped reduce soot forming intermediates including ben-
 32 zene, cyclopentadienyl, acetylene, propargyl, and vinylacetylene [13]. Hayes
 33 and Burgess [14] computationally examined the peroxy radical isomerization
 34 reactions for MV to better understand the low temperature reaction pathways.
 35 Finally, Diévert et al. [15] used diffusion flames in the counterflow configuration
 36 to determine extinction limits for a number of methyl esters, including MV, and
 37 validated a detailed kinetic model with the experimental data.

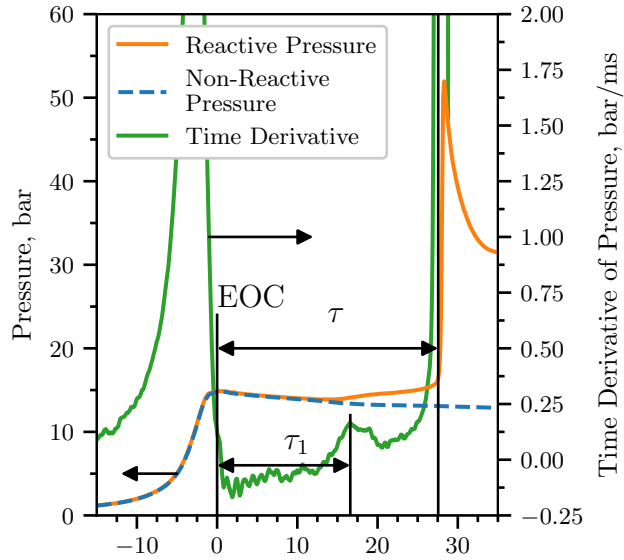
38 This work provides additional data for the autoignition of MV. Data is col-
 39 lected in a RCM under engine relevant conditions spanning from 15 bar to 30 bar,
 40 equivalence ratios (ϕ) from 0.25 to 2.0, and temperatures from 680 K to 1050 K.
 41 The NTC region of MV is mapped out to provide additional information on the
 42 fidelity of using MV as a biodiesel surrogate [and insights into the autoignition](#)
 43 [chemistry of large methyl esters](#).

44 2. Experimental Methods

45 The RCM used in this study is a single piston arrangement and is pneu-
 46 matically driven and hydraulically stopped. The device has been described in
 47 detail previously [16] and will be described here briefly for reference. The end
 48 of compression (EOC) temperature and pressure (T_C and P_C respectively), are
 49 independently changed by varying the overall compression ratio, initial pressure
 50 (P_0), initial temperature (T_0), and specific heat ratio of the experiments. The
 51 piston in the reaction chamber is machined with a specially designed crevice to
 52 suppress the roll-up vortex effect and promote homogeneous conditions in the
 53 reactor during and after compression [17].

54 The primary diagnostic on the RCM is the in-cylinder pressure measured by

55 a Kistler 6125C dynamic transducer that is compensated for thermal shock. The
 56 transducer is coupled to a Kistler 5010B charge amplifier. The voltage output
 57 of the charge amplifier is recorded by a National Instruments 9125 analog input
 58 device connected to a cDAQ 9178 chassis. The voltage is sampled at a rate of
 59 either 50 kHz or 100 kHz by a LabView VI and processed by a Python package
 60 called UConnRCMPy [18]. Version 3.0.5 of UConnRCMPy [19], 3.6 of Python,
 61 2.3.0 of Cantera [20], 1.13.0 of NumPy [21], 0.19.0 of SciPy [22], and 2.0.1 of
 62 Matplotlib [23] are used in the analysis in this paper.



63

Figure 1: Definition of the ignition delays used in this work. The experiment in this figure is
 conducted for a $\phi = 2.0$ mixture with $\text{Ar}/(\text{N}_2 + \text{Ar}) = 0.5$, $P_0 = 0.7806$ bar, $T_0 = 373$ K, $P_C =$
 14.92 bar, $T_C = 720$ K, $\tau = (27.56 \pm 0.89)$ ms, and $\tau_1 = (16.60 \pm 0.46)$ ms. [The non-reacting](#)
 64 [pressure trace by replacing \$\text{O}_2\$ with \$\text{N}_2\$ is also shown for reference.](#)

65 The compression stroke of the RCM brings the fuel/oxidizer mixture to the
 66 EOC conditions, and for suitable thermodynamic states, the mixture will ignite
 67 after a delay period. The definitions of the ignition delays are shown in Fig. 1.
 68 The time of the EOC is defined as the maximum of the pressure trace prior to
 69 the start of ignition and the ignition delays are defined as the time from the EOC

until local maxima in the first time derivative of the pressure. Each experimental condition is repeated at least five times to ensure repeatability of the data. As there is some random scatter present in the data, the standard deviation (σ) of the ignition delays from the runs at a given condition is computed. Typically, σ is less than 10 % of the mean values of the overall ignition delay (τ) and the first stage ignition delay (τ_1).

In addition to the reactive experiments, non-reactive experiments are conducted by replacing O_2 with N_2 to determine the influence of machine-specific behavior on the experimental conditions (see Fig. 1) and permit the calculation of the EOC temperature via the isentropic relations between pressure and temperature [24]. The EOC temperature is calculated by the procedure described in Section 3.

The mixtures considered in this study are shown in Table 1. Four equivalence ratios of MV in “air” are considered. While O_2 is kept at 21 % by mole in the oxidizer, the ratio of Ar : N_2 in the oxidizer is varied to adjust the temperatures reached at the EOC. Two P_C conditions are studied in this work, 15 bar and 30 bar, representing engine-relevant conditions. For the $\phi = 2.0$ condition, only $P_C = 15$ bar is considered because we could not achieve T_C values low enough that the ignition during the compression stroke can be prevented.

Table 1: Mixtures considered in this work

| ϕ | Mole Fraction (purity) | | | | Ar/($N_2 + Ar$) |
|--------|------------------------|------------------|---------------|------------------|-------------------|
| | MV (100 %) | O_2 (99.994 %) | Ar (99.999 %) | N_2 (99.999 %) | |
| 0.25 | 0.0065 | 0.2087 | 0.7848 | 0.0000 | 1.0 |
| 0.5 | 0.0130 | 0.2074 | 0.7796 | 0.0000 | 1.0 |
| 1.0 | 0.0256 | 0.2047 | 0.7697 | 0.0000 | 1.0 |
| 1.0 | 0.0256 | 0.2047 | 0.3849 | 0.3848 | 0.5 |
| 2.0 | 0.0499 | 0.1996 | 0.0000 | 0.7505 | 0.0 |
| 2.0 | 0.0499 | 0.1996 | 0.3752 | 0.3753 | 0.5 |

Mixtures are prepared in stainless steel mixing tanks, 17 L and 15 L in size. The proportions of reactants in the mixture are determined by specifying the absolute mass of the fuel, the equivalence ratio, and the ratio of Ar : N₂ in the oxidizer. Mixtures are made by first vacuuming the mixing tanks to an ultimate pressure less than 5 Torr. Since MV is a liquid with a relatively small vapor pressure at room temperature and pressure, it is measured gravimetrically to within 0.01 g of the specified value. The fuel is injected into the mixing tank through a septum. Proportions of O₂, Ar, and N₂ are added manometrically at room temperature and the total pressure is measured by an Omega Engineering MMA100V10T2D0T4A6 type static pressure transducer. The same transducer is used to measure the pressure of the ~~reactants~~ reactant mixture prior to an experiment.

The RCM is equipped with heaters to control the initial temperature of the mixture. After filling in the components to the mixing tanks, the heaters are switched on and the system is allowed 1.5 h to come to steady state. The mixing tanks are also equipped with magnetic stir bars so the reactants are well mixed for the duration of the experiments. Previous work has shown this procedure to completely vaporize the fuel and prevent fuel cracking during the heating process [25–27].

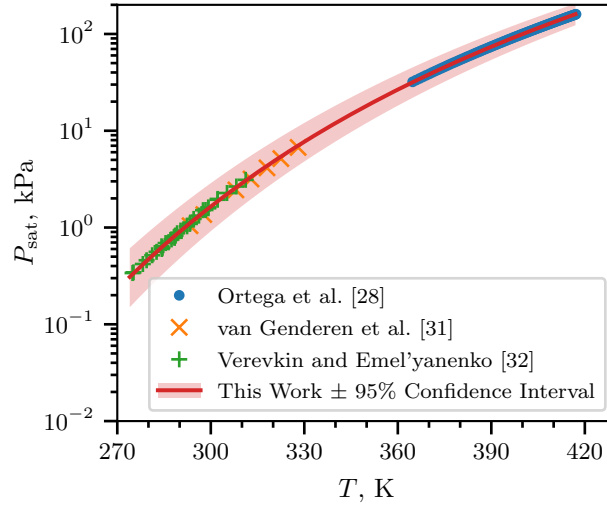
~~Saturated vapor pressure of MV as a function of temperature, plotted using the Antoine equation, Eq. (1), with $A = 6.4030$, $B = 1528.69$, and $C = 52.881$.~~

The initial temperature is chosen such that the saturated vapor pressure (P_{sat}) of the fuel at the initial temperature is at least twice the partial pressure of the fuel in the mixing tank. The Antoine equation

$$\log_{10} P_{\text{sat}} = A - \frac{B}{T - C} \quad (1)$$

is used to model the saturated vapor pressure of MV as a function of temperature (T), where A , B , and C are substance-specific coefficients, given in units of K and kPa. Coefficients for Eq. (1) are given in the literature by Ortega et al. [28], Camacho et al. [29], and Stephenson et al. [30]. Unfortunately, the values of the coefficients are different among all three references. Therefore, coefficients for

119 use in Eq. (1) are determined in this work by least squares fitting of the data
 120 of Ortega et al. [28], van Genderen et al. [31], and Verevkin and Emel'yanenko
 121 [32] using the `curve_fit()` function of SciPy [22] version 0.19.0. Figure 2
 122 shows that the coefficients fitted with this procedure give good agreement with
 123 the experimental data; values for the coefficients computed in this work and
 124 [reported](#) in the literature works are given in Table 2. The data and code used
 125 to calculate the coefficients are provided in the Supplementary Material.



126

Figure 2: [Saturated vapor pressure of MV as a function of temperature, plotted using the Antoine equation, Eq. \(1\), with \$A = 6.4030\$, \$B = 1528.69\$, and \$C = 52.881\$.](#)

Table 2: Antoine Equation coefficients computed in this work and [obtained](#) from the literature, [in units of K and kPa](#). The 2σ confidence interval is estimated by taking the square root of the diagonals of the covariance matrix returned from `curve_fit()`

128

| | A | B | C | T_{\min} , K | T_{\max} , K |
|--------------------------------|---------|---------|--------|----------------|----------------|
| This Work | 6.4030 | 1528.69 | 52.881 | 274.9 | 417.18 |
| 2 σ Confidence Interval | 0.0919 | 53.47 | 4.934 | — | — |
| Ortega et al. [28] | 6.23175 | 1429.00 | 62.30 | 364.75 | 417.18 |
| Camacho et al. [29] | 5.9644 | 1281.06 | 75.94 | 281 | 547 |
| Stephenson et al. [30] | 6.62646 | 1658.4 | 42.09 | 297 | 411 |

3. Computational Methods

3.1. RCM Modeling

The Python 3.6 interface of Cantera [20] version 2.3.0 is used for all simulations in this work. Detailed descriptions of the use of Cantera for these simulations can be found in the work of Weber and Sung [18] and Dames et al. [33]; a brief overview is given here. As mentioned in Section 2, non-reactive experiments are conducted to characterize the machine-specific effects on the experimental conditions in the RCM. This pressure trace is combined with the reactive pressure trace and used to compute a volume trace by assuming that the reactants undergo a reversible, adiabatic, constant composition (i.e., isentropic) compression during the compression stroke and an isentropic expansion after the EOC. The volume trace is applied to a simulation conducted in an `IdealGasReactor` in Cantera [20] using the CVODES solver from the SUNDIALS suite [34]. The ignition delays from the simulations are defined in the same manner as in the experiments. The time derivative of the pressure in the simulation is computed by second order Lagrange polynomials, as discussed by Chapra and Canale [35]. The volume trace files, the corresponding pressure traces, and `volume-trace.yaml` files suitable for use with UConnRCMPy v3.0.5 [19] are available on the web at <https://combdialab.engr.uconn.edu/database/rcm-database> and on figshare at <https://doi.org/10.6084/m9.figshare.5213341>. In addition, ChemKED-format [36] files are available in the main ChemKED database repository at <https://github.com/pr-ometh-us/ChemKED-database>.

153 To the best of our knowledge, there are three mechanisms for MV com-
 154 bustion available in the literature. The first two, by Korobeinichev et al. [12]
 155 and Dmitriev et al. [13], were developed to simulate flames, and do not include
 156 the low-temperature chemistry necessary to simulate the conditions in ~~these~~ the
 157 current RCM experiments. The third model was developed by Diévaré et al. [15]
 158 and includes low-temperature chemistry of MV, although it was only validated
 159 by comparison with flame extinction limits. In converting this mechanism for
 160 use in Cantera, we found that there were many species in the thermodynamic
 161 database with multiple data entries. For most of these species the thermody-
 162 namic data is identical. However, some species are not exact duplicates. For
 163 these species, it is not clear from the thermodynamic database file which data set
 164 should be preferred. Since Cantera (and CHEMKIN) choose the first instance
 165 of a duplicate species to be used, we retained the first entry for all duplicated
 166 species. The detailed model of Diévaré et al. [15] includes 1105 species and 7141
 167 reactions, and the Cantera formatted input file is available in the Supplementary
 168 Material.

169 3.2. Reaction Mechanism Generator

170 In addition to using a mechanism from the literature, we investigate the
 171 use of an automatic mechanism generator, the open-source Reaction Mecha-
 172 nism Generator (RMG) [37] version 2.1.0. The Python version of RMG is used,
 173 which requires Python 2.7, and version 2.1.0 of the RMG database is used.
 174 The final RMG model contains 427 species and 13640 reactions. Note that the
 175 number of species is much lower than the Diévaré et al. [15] model because the
 176 RMG model focuses on only one fuel (MV), but the number of reactions is sub-
 177 stantially higher. The input file used to generate the model is available in the
 178 Supplementary Material. In addition, the CHEMKIN and Cantera formatted
 179 input files for the ~~RMG~~ RMG-generated model are available in the Supplemen-
 180 tary Material.

181 4. Experimental Results

182 4.1. Ignition Delays

183 Figure 3 shows the ignition delay results measured in this study. Filled mark-
184 ers denote the overall ignition delay and hollow markers indicate the first-stage
185 ignition delay. Vertical error bars are drawn on the symbols to represent the 2σ
186 uncertainty in the ignition delay; for many of the experiments, the uncertainty
187 is approximately the same size as the data point, so the error bar is hidden.
188 Horizontal error bars are shown on the first and last points of each equivalence
189 ratio indicating the estimated uncertainty in the EOC temperature of $\pm 1\%$ [38].
190 Fig. 3a shows the results for a compressed pressure of 15 bar, while Fig. 3b shows
191 the results for a compressed pressure of 30 bar. Note that $\phi = 2.0$ results were
192 not collected for 30 bar, so there are no red triangle data points in Fig. 3b. A
193 summary of the ignition delay data is available as a comma-separated value
194 file in the Supplementary Material, [including the mixture conditions for each](#)
195 [experiment, the initial conditions, the compressed conditions, and the ignition](#)
196 [delays and their associated errors.](#)

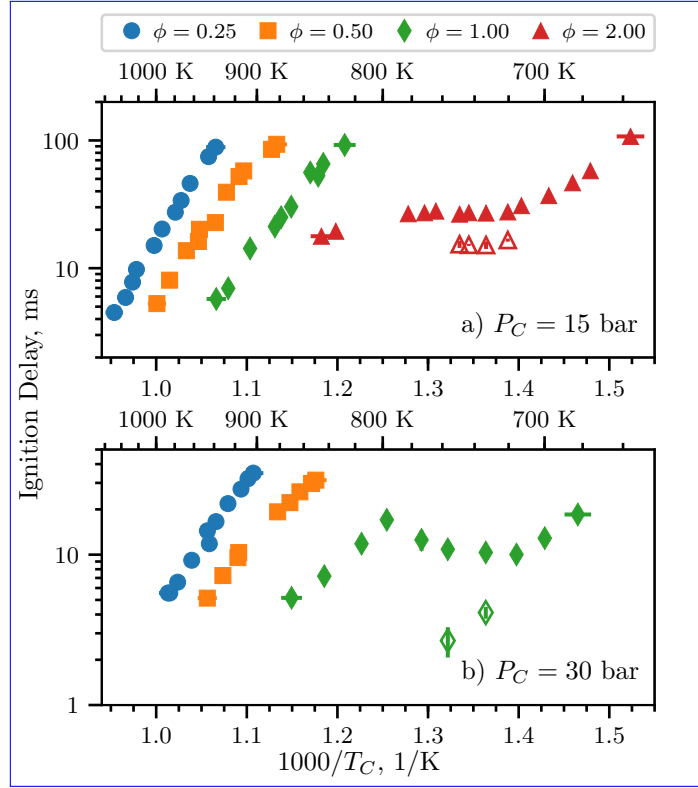


Figure 3: Ignition delays of MV as a function of inverse temperature for varying equivalence ratios. Filled points are the overall ignition delays and hollow points are the first stage ignition delays. a) 15 bar, b) 30 bar.

It can be seen from Fig. 3 that the ignition delays for the $\phi = 0.25$ and 0.5 mixtures do not show an NTC region of the ignition delay for both of the pressures studied in this work. However, the $\phi = 1.0$ mixture shows an NTC region at $P_C = 30$ bar between approximately 720 K and 800 K, with measured first-stage ignition delays at 733 K and 757 K. In addition, the $\phi = 2.0$ mixture shows an NTC region of ignition delay at 15 bar from approximately 720 K to 780 K, with measured first-stage ignition delays between 720 K and 750 K.

~~Ignition delays of MV as a function of inverse temperature for varying equivalence ratios. Filled points are the overall ignition delays and hollow points are the first stage ignition delays. a) 15 bar, b) 30 bar.~~

Hadj-Ali et al. [9] also observed two-stage ignition of MV in stoichiometric

210 mixtures, stating that “[m]ethyl pentanoate... was more reactive [than methyl
 211 butanoate] with a limit below which autoignition no longer occurs observed at
 212 $T_c = 670$ K and $P_c = 11.4$ bar. At this temperature, the autoignition occurred
 213 in two stages with a clearly identified cool flame event.” However, we do not
 214 find ~~two-stage~~ two-stage ignition for the similar pressure of $P_C = 15$ bar in
 215 this study. We note that the stated temperature of the experiment from the
 216 work of Hadj-Ali et al. [9] (670 K) is much lower than the lowest temperature
 217 we considered in this work at 15 bar, $\phi = 1.0$ (828 K). We did not conduct
 218 experiments at lower temperatures because the work of Mittal and Sung [17]
 219 showed that the temperature field in the RCM reaction chamber was uniform
 220 for approximately 100 ms after the EOC, and our measured ignition delay at
 221 15 bar, $\phi = 1.0$, and 828 K is 92.14 ms.

222 However, we ~~note~~ find NTC behavior of the overall ignition delay and two-
 223 stage ignition at the higher pressure of 30 bar, and at higher temperatures than
 224 those reported for two-stage ignition in the study of Hadj-Ali et al. [9]. The
 225 trend of NTC behavior shifting to higher temperatures with increasing pressure
 226 can be seen in other classes of fuels. Kukkadapu et al. [39] found a similar
 227 trend in gasoline composed of iso-alkanes, n-alkanes, cyclo-alkanes, aromatics,
 228 and olefins. Kukkadapu et al. [39] attributed the shift of the NTC region to the
 229 reactions between the hydroperoxyalkyl radical (QOOH) and O_2 becoming more
 230 dominant than the unimolecular decomposition of QOOH at higher pressures.
 231 Similar trends could occur for the hydroperoxyalkyl radicals of MV.

232 To further understand the effect of the methyl ester functional group on the
 233 NTC region of ignition delay, we compare with the alkane and alcohol with
 234 5-carbon alkyl chains, n-pentane and n-pentanol. n-Pentane and MV have the
 235 same fuel mole percentage for stoichiometric mixtures in air (2.56 %), while
 236 n-pentanol has a fuel mole percentage of 2.72 % for stoichiometric conditions.
 237 Ribaucour et al. [40] and Bugler et al. [41] found the NTC region for n-pentane
 238 to be between 760 K and 910 K at pressures near 10 atm. As we will compare
 239 with our MV data at 30 bar, we note that increasing the pressure tends to shift
 240 the NTC to higher temperatures, as mentioned previously [39]. Heufer et al. [42]

found NTC behavior for n-pentanol in the range of 770 K to 900 K at 30 bar. In this study, we find the NTC window for MV at 30 bar to be between 720 K and 800 K. Therefore, it appears that the methyl ester functional group causes the NTC range to occur at lower temperature as compared to alkanes and alcohols with similar alkyl chain lengths. This result was also noted by Hadj-Ali et al. [9] for methyl hexanoate as the fuel.

4.2. Pressure Traces

Figure 4a shows the pressure traces for selected experiments at $\phi = 1.0$, $P_C = 30$ bar. The three reactive pressure traces shown are at the low-temperature end of the NTC (blue, 700 K), one case with two-stage ignition (orange, 733 K), and one case near the high-temperature limit of the NTC region (green, 774 K). Also shown is the non-reactive pressure trace for the 700 K case (red). By comparing the 700 K pressure trace with the non-reactive pressure trace, it can be seen that there is substantial heat release prior to main ignition as measured by the deviation of the reactive pressure trace from the non-reactive trace. However, there is only one peak in the time derivative of the pressure, so no first-stage ignition delay is defined for this case. It can also be seen in Fig. 4a that the 774 K case shows some heat release prior to ignition, although again there is only one peak in the time derivative of the pressure. Furthermore, the heat release at 774 K appears to be more gradual than at 700 K.

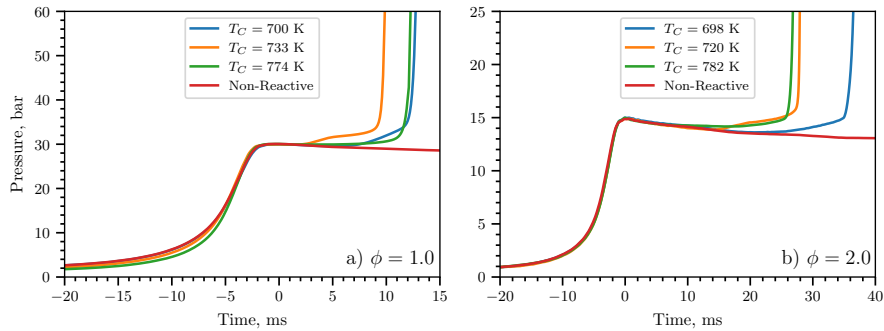


Figure 4: Selected pressure traces around the NTC region of ignition delay. a) $\phi = 1.0, P_C = 30 \text{ bar}$ $\phi = 1.0, P_C = 30 \text{ bar}$, b) $\phi = 2.0, P_C = 15 \text{ bar}$ $\phi = 2.0, P_C = 15 \text{ bar}$.
The corresponding non-reactive pressure traces are also included for reference.

A similar trend can be observed in Fig. 4b for $\phi = 2.0$ at $P_C = 15 \text{ bar}$, where pressure traces at several points around the NTC region are plotted. As in Fig. 4a, the three reactive pressure traces shown are at the low-temperature end of the NTC (blue, 698 K), one case with two-stage ignition (orange, 720 K), and one case near the high-temperature limit of the NTC region (green, 782 K). Also shown is the non-reactive pressure trace for the 698 K case (red). As for the $\phi = 1.0$ case, the pressure traces show significant heat release prior to the overall ignition, as judged by deviation from the non-reactive case.

5. Computational Results

Figure 5 compares experimentally measured overall ignition delays with ignition delays computed with the detailed model of Diévar et al. [15] (solid lines). Figure 5a shows results at $P_C = 15 \text{ bar}$, while Fig. 5b shows results at $P_C = 30 \text{ bar}$. Only some equivalence ratios are shown for each pressure condition; data and simulated results are not shown for cases where the reactive simulated temperature at the EOC deviated substantially from the non-reactive temperature due to heat release during the compression stroke. Furthermore, it is important to note that the model of Diévar et al. [15] was not validated for MV ignition delays, only for extinction strain rates.

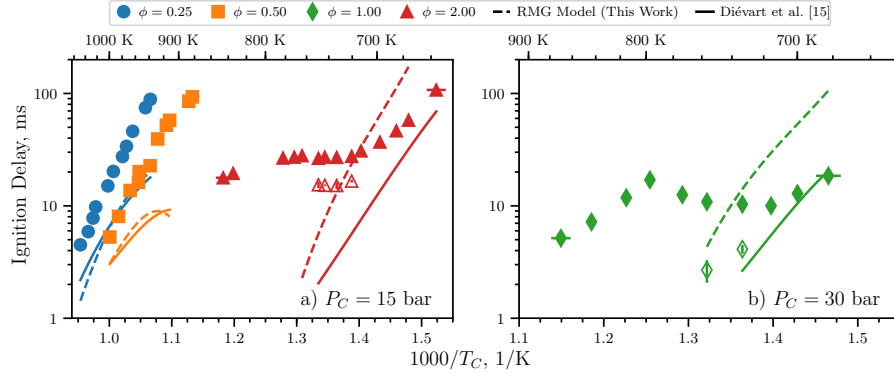


Figure 5: Comparison of experimental (τ) and simulated (τ) ignition delays computed using the procedure described in Section 3.1. a) 15 bar, b) 30 bar.

At 15 bar, the experimental overall ignition delays are under-predicted by the Diévert et al. [15] model for the three equivalence ratios shown. For the $\phi = 0.25$ and 0.5 conditions, the model appears to be predicting an NTC region of the overall ignition delays as the temperature decreases, as judged by the increasing curvature of the simulations, although such a trend is not observed in the for the experimental data. However, at $\phi = 2.0$, the model does not predict the presence of an NTC region, although one is present in the experiments. Nonetheless, the agreement seems to be improving as the temperature is decreased. Comparing the Diévert et al. [15] model to the stoichiometric data at 30 bar, we find a similar trend as the $\phi = 2.0, P_C = 15 \text{ bar}$ data. The model does not predict the NTC region found experimentally for the $\phi = 1.0, P_C = 30 \text{ bar}$ experiments, but the agreement improves as the temperature decreases. Interestingly, two-stage ignition is predicted for all of the $\phi = 1.0$ and $\phi = 2.0$ data shown in Fig. 5. However, the first-stage ignition delays are 0.1 ms to 0.5 ms less than the overall ignition delays, and are not shown on Fig. 5 because they are nearly indistinguishable from the overall ignition delay. While

To further understand the model of Diévert et al. [15] over-predicts the first-stage ignition delay, we have conducted adiabatic, constant volume simulations (called CONV simulations), as these simulations are not linked to a particular

experiment by the volume trace and can be conducted over a wide range of temperatures. In the CONV simulations, overall ignition delay is defined as an increase in the temperature of 400 K over the initial temperature. The diluent for all of the CONV simulations is pure argon, although the RCM simulations described previously consider the diluent mixture associated with each experiment (either pure argon or a 50:50 mixture of argon and nitrogen by mole, see Table 1 and the Supplementary Material).

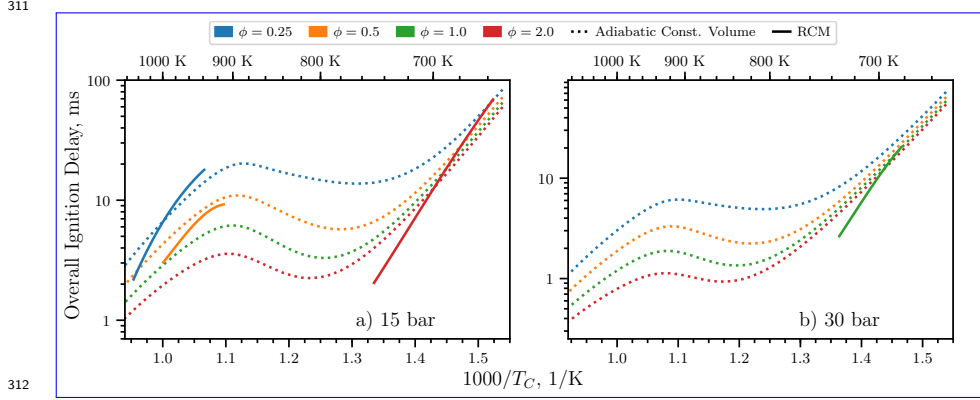


Figure 6: Comparison of simulated overall ignition delays computed in an adiabatic, constant volume system (dotted lines) and computed using the procedure described in Section 3.1 (solid lines). a) 15 bar, b) 30 bar.

Figure 6 compares the CONV simulations to the RCM simulations shown in Fig. 5. From Fig. 6, it can be seen that the curvature in the RCM simulations at $P_C = 15$ bar, $\phi = 0.25$ and 0.5 is related to the NTC region of the overall ignition delay, while the lack of curvature in the $P_C = 15$ bar, $\phi = 2.0$ and the $P_C = 30$ bar, $\phi = 1.0$ simulations is because those lie on the low-temperature side of the predicted NTC. It is clear from Fig. 6 that the model of Diévert et al. [15] predicts the NTC to occur at too high a temperature relative to the experiments.

To elucidate the underlying reasons for the disagreement between the Diévert et al. [15] model and the data, we constructed conduct simulations with an ad-

ditional model constructed using RMG (see Section 3.2). As can be seen in Fig. 5a, the agreement between the RMG model (dashed lines) and the experimental data is similar to the Diévert et al. [15] model for the ~~15-bar~~ $P_C = 15$ bar, $\phi = 0.25$ and 0.5 data. Moreover, the RMG model predicts a similar NTC region as temperature is decreasing. For the ~~15-bar~~ $P_C = 15$ bar, $\phi = 2.0$ data, the RMG model tends to over-predict the low-temperature ~~ignition delays, overall~~ignition delays (i.e., those to the right of the experimental NTC region on the Arrhenius plot), and does not predict the NTC region found experimentally. As before, the trend at ~~30-bar~~ $P_C = 30$ bar, $\phi = 1.0$ is similar to the ~~15-bar~~ $P_C = 15$ bar, $\phi = 2.0$ data; the RMG model over-predicts the low-temperature overall ignition delays and does not predict the experimental NTC region. Finally, as in the Diévert et al. [15] model, two-stage ignition is predicted for all of the $\phi = 1.0$ and $\phi = 2.0$ data shown in Fig. 5. However, the first-stage ignition delays are 0.1 ms to 0.5 ms less than the overall ignition delays, and are not shown on Fig. 5 because they are nearly indistinguishable from the overall ignition delay. ~~Again, the over-prediction of the first-stage ignition delay and pressure rise requires further investigation and understanding of the complex low-temperature chemistry.~~

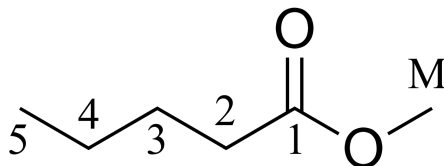
It is clear that neither model is able to predict the ignition delays of MV particularly well. In addition to the poor agreement shown in Fig. 5, the simulations for $P_C = 15$ bar, $\phi = 1.0$ and $P_C = 30$ bar, $\phi = 0.25, 0.5$ and 2.0 showed substantial heat release during the compression stroke (i.e., the simulations are much too reactive), and so these conditions ~~aren't~~are not compared in Fig. 5. We note again that the model by Diévert et al. [15] was validated for MV combustion only by comparison to flame extinction limits, so the disagreement is not wholly surprising.

In general, there could be three likely sources of error in the models: missing reaction pathways, incorrect values of the reaction rates, and incorrect values for thermodynamic properties of the species. We have noted in Section 3.2 that the RMG model has many more reactions than the Diévert et al. [15] model and the algorithm used in RMG considers a substantial number of the possible

pathways. This reduces the possibility of missing reaction pathways affecting the model. Further detailed studies are required to ensure that the RMG model includes all of the relevant reaction pathways, which are outside the scope of this work.

The second source of error may be incorrect reaction rate parameters, either because the rates are specified incorrectly in the model or because the rates are not well estimated by the typical analogy based-rules. It should be noted that errors of this type may affect the model generated by RMG—if the rates are not estimated correctly, reactions that are important in reality may not be included in the model. Determining the accuracy of the reaction rates used in the RMG and Diévar et al. [15] models requires further detailed studies of the models, which are also outside the scope of this work. Another, related, source of error could be incorrect estimation of the pressure dependence of the reaction rates, which may be particularly important for the isomerization reactions prevalent in low-temperature chemistry.

The third source of error may lie in the estimation of the thermodynamic properties of the species, particularly the fuel radicals. In the work of Diévar et al. [15], the program THERM~~[43]~~[43] was used to estimate thermodynamic values using the group additivity method. In the RMG model constructed in this work, RMG itself estimates the thermodynamic properties of the molecules also using the group additivity method. Nonetheless, the two models have differing predictions of the thermodynamic properties of the species in the model, particularly the fuel and its radicals. The values of the heats of formation of the fuel and its H-atom abstraction radicals are shown in Table 3; the radicals are labeled according to the convention shown in Fig. 7.



381

Figure 7: Structure of MV with carbon atoms labeled according to the convention used in

Table 3 and Table 4

Table 3 shows that the heats of formation of the fuel and radicals 3, 4, 5, and M are quite similar between the two mechanisms. However, the heat of formation of the second radical, the one closest to the methyl ester group, has a significantly lower heat of formation in the model by Diévert et al. [15] than in the RMG model. Note that it is expected that the second radical will be somewhat more stable than the other radicals, due to the influence of the methyl ester group on the adjacent carbon atom.

Table 3: Heats of formation of MV and its radicals, labeled according to the convention used in Fig. 7

| Radical Site | Diévert et al. [15] | | RMG Model (this work) | |
|--------------|---------------------|------------|-----------------------|------------|
| | [kJ/mol] | [kcal/mol] | [kJ/mol] | [kcal/mol] |
| MV | -470.98 | -112.57 | -472.53 | -112.94 |
| 2 | -297.16 | -71.02 | -273.63 | -65.40 |
| 3 | -277.03 | -66.21 | -273.63 | -65.40 |
| 4 | -277.03 | -66.21 | -278.61 | -66.59 |
| 5 | -265.94 | -63.56 | -267.53 | -63.94 |
| M | -270.51 | -64.65 | -270.12 | -64.56 |

~~Table 3 shows that the heats of formation of the fuel and radicals 3, 4, 5, and M are quite similar between the two mechanisms. However, the heat of formation of the second radical, the one closest to the methyl ester group, has a significantly lower heat of formation in the model by Diévert et al. [15] than in the RMG model. Note that it is expected that the second radical will be somewhat more stable than the other radicals, due to the influence of the methyl ester group on the adjacent carbon atom.~~

This difference in heats of formation affects the pathways that consume the fuel. By conducting a reaction pathway analysis to determine which radicals are formed from the breakdown of the fuel, we can analyze the proportion of each

radical formed as the fuel breaks down during the autoignition process. The following analysis is conducted for a constant volume, adiabatic simulation with initial temperature and pressure of 700 K, ~~30 bar, and 30 bar, respectively,~~ and for the stoichiometric equivalence ratio. The rates of production of the species have been integrated until the time of 20 % fuel consumption. The results of this analysis are shown in Table 4 for the two models. The percentages shown in ~~the~~ Table 4 are the percent of the fuel consumed to form a particular fuel radical by all the reactions that can form that radical, and the radicals are labeled according to the convention in Fig. 7.

~~Percent of MV consumed to form fuel radical species with a hydrogen atom missing at the location indicated in the first column and Fig. 7 Radical Site~~
~~Diévar et al. [15] %RMG Model %RMG switched %2 29.2 12.5 11.0 3 17.5 12.2~~
~~11.1 4 17.5 50.6 56.6 5 9.5 3.9 4.3 M 26.3 20.8 16.9~~

At the relatively low temperature and high pressure condition of this analysis, all of the fuel is consumed by H-atom abstractions to form the fuel radicals shown. It can be seen that the two models have quite different distributions of products from the first H-abstraction reactions. The model of ~~[15]~~ Diévar et al. [15] predicts that H-abstraction from the second carbon is the most prevalent, while the RMG model predicts that the radical on the fourth carbon in the chain will be primarily formed. This is in line with the heats of formation in Table 3, where the most stable radical (i.e., the radical with the smallest heat of formation) is most likely to be formed in each model.

Table 4: Percent of MV consumed to form fuel radical species with a hydrogen atom missing at the location indicated in the first column and Fig. 7

| Radical Site | Diévert et al. [15] [%] | RMG Model [%] | RMG switched [%] |
|--------------|-------------------------|---------------|------------------|
| 2 | 29.2 | 12.5 | 11.0 |
| 3 | 17.5 | 12.2 | 11.1 |
| 4 | 17.5 | 50.6 | 56.6 |
| 5 | 9.5 | 3.9 | 4.3 |
| M | 26.3 | 20.8 | 16.9 |

To further compare the models with each other, the NASA polynomials representing the thermodynamic properties of MV and the 5 fuel radicals from the model of Diévert et al. [15] ~~and~~ are used to replace the equivalent molecules in the RMG model. The results of a path analysis at the same condition as the other analysis is shown in Table 4 in the “RMG switched” column. ~~This analysis shows~~ The results of the analysis of the “RMG switched” model show that the radical on the fourth carbon ~~atom~~ is still the most ~~prevalant, despite changing prevalent, despite~~ the heats of formation ~~of the fuel and its radicals, for the fuel radicals in the “RMG switched” model being identical to the Diévert et al. [15] model.~~ This suggests that the reaction pathways have a substantial impact on the simulation, in addition to the influence of the thermochemistry, as discussed previously. Moreover, since the thermochemistry of the species in a reaction controls the reverse reaction rate of a reaction, the RMG algorithm may miss important pathways due to improperly estimated thermochemistry.

Taken together, these results show that the poor performance in a given model cannot be attributed to a single source. ~~There is a strong interaction between the thermodynamics of the species and the kinetics of the reactions, requiring~~ Separating the influence of thermochemistry and kinetics requires further detailed study of the methyl ~~ester system~~ valerate system specifically, and methyl ester systems more generally. Although such detailed work has begun, for example, with the work of Hayes and Burgess [14], further work is required to accurately predict the low temperature ignition delays of methyl valerate.

449 6. Conclusions

450 In this study, we have measured ignition delays for methyl valerate over a
451 wide range of engine-relevant pressures, temperatures, and equivalence ratios.
452 An NTC region of the [overall](#) ignition delay and two-stage ignition are recorded
453 for pressures of 15 bar at $\phi = 2.0$ and 30 bar at $\phi = 1.0$. A detailed chemical
454 kinetic model available in the literature is unable to reproduce the experimental
455 results, so a new model is constructed using the Reaction Mechanism Generator
456 software. Although the new model contains many more reactions than the
457 literature model, it is still unable to predict the experimental ignition delays
458 satisfactorily. Both models predict an NTC region of the [overall](#) ignition delay
459 under conditions where none is found in the experiments, and fail to predict
460 the NTC region of [overall](#) ignition delay that is present in the experiments.
461 Possible reasons for the discrepancy include missing reaction pathways, incorrect
462 rate estimates, and incorrect thermodynamic property estimates. Comparative
463 analysis of the two models failed to identify a single source of the error, and
464 further detailed studies are required to improve predictions of the ignition delay
465 at these engine-relevant conditions.

466 7. Acknowledgments

467 The authors acknowledge support from the Combustion Energy Frontier
468 Research Center, an Energy Frontier Research Center funded by the U.S. De-
469 partment of Energy, Office of Science, Office of Basic Energy Sciences, under
470 award number DE-SC0001198.

471 References

- 472 [1] S. K. Hoekman, C. Robbins. Review of the effects of biodiesel
473 on NOx emissions. Fuel Processing Technology 96 (2012) 237–249.
474 doi:10.1016/j.fuproc.2011.12.036.

- 475 [2] J. Y. Lai, K. C. Lin, A. Violi. Biodiesel combustion: Advances in chemical
476 kinetic modeling. *Progress in Energy and Combustion Science* 37 (2011)
477 1–14. doi:10.1016/j.pecs.2010.03.001.
- 478 [3] L. Coniglio, H. Bennadji, P. Glaude, O. Herbinet, F. Billaud. Combustion
479 chemical kinetics of biodiesel and related compounds (methyl and
480 ethyl esters): Experiments and modeling – Advances and future refinements.
481 *Progress in Energy and Combustion Science* 39 (2013) 340–382.
482 doi:10.1016/j.pecs.2013.03.002.
- 483 [4] W. K. Metcalfe, S. Dooley, H. J. Curran, J. M. Simmie, A. M. El-Nahas,
484 M. V. Navarro. Experimental and modeling study of C₅H₁₀O₂ ethyl and
485 methyl esters. *The Journal of Physical Chemistry A* 111 (2007) 4001–4014.
486 doi:10.1021/jp067582c.
- 487 [5] S. M. Walton, M. S. Wooldridge, C. K. Westbrook. An experimental
488 investigation of structural effects on the auto-ignition properties of two
489 C₅ esters. *Proceedings of the Combustion Institute* 32 (2009) 255–262.
490 doi:10.1016/j.proci.2008.06.208.
- 491 [6] S. Dooley, H. J. Curran, J. M. Simmie. Autoignition mea-
492 surements and a validated kinetic model for the biodiesel surro-
493 gate, methyl butanoate. *Combustion and Flame* 153 (2008) 2–32.
494 doi:10.1016/j.combustflame.2008.01.005.
- 495 [7] B. Akih-Kumgeh, J. M. Bergthorson. Comparative Study of Methyl Bu-
496 tanoate and n -Heptane High Temperature Autoignition. *Energy & Fuels*
497 24 (2010) 2439–2448. doi:10.1021/ef901489k.
- 498 [8] B. Akih-Kumgeh, J. M. Bergthorson. Structure-reactivity trends of C₁–C₄
499 alkanolic acid methyl esters. *Combustion and Flame* 158 (2011) 1037–1048.
500 doi:10.1016/j.combustflame.2010.10.021.
- 501 [9] K. Hadj-Ali, M. Crochet, G. Vanhove, M. Ribaucour, R. Minetti. A study

- of the low temperature autoignition of methyl esters. *Proceedings of the Combustion Institute* 32 (2009) 239–246. doi:10.1016/j.proci.2008.09.002.
- [10] K. Kumar, C.-J. Sung. Autoignition of methyl butanoate under engine relevant conditions. *Combustion and Flame* 171 (2016) 1–14. doi:10.1016/j.combustflame.2016.04.011.
- [11] E. Fisher, W. J. Pitz, H. J. Curran, C. K. Westbrook. Detailed chemical kinetic mechanisms for combustion of oxygenated fuels. *Proceedings of the Combustion Institute* 28 (2000) 1579–1586. doi:10.1016/S0082-0784(00)80555-X.
- [12] O. Korobeinichev, I. Gerasimov, D. Knyazkov, A. Shmakov, T. Bolshova, N. Hansen, C. K. Westbrook, G. Dayma, B. Yang. An Experimental and Kinetic Modeling Study of Premixed Laminar Flames of Methyl Pentanoate and Methyl Hexanoate. *Zeitschrift für Physikalische Chemie* 229 (2015). doi:10.1515/zpch-2014-0596.
- [13] A. M. Dmitriev, D. A. Knyazkov, T. A. Bolshova, A. G. Shmakov, O. P. Korobeinichev. The effect of methyl pentanoate addition on the structure of premixed fuel-rich n-heptane/toluene flame at atmospheric pressure. *Combustion and Flame* 162 (2015) 1964–1975. doi:10.1016/j.combustflame.2014.12.015.
- [14] C. Hayes, D. R. Burgess. Exploring the oxidative decompositions of methyl esters: Methyl butanoate and methyl pentanoate as model compounds for biodiesel. *Proceedings of the Combustion Institute* 32 (2009) 263–270. doi:10.1016/j.proci.2008.05.075.
- [15] P. Diévert, S. H. Won, J. Gong, S. Dooley, Y. Ju. A comparative study of the chemical kinetic characteristics of small methyl esters in diffusion flame extinction. *Proceedings of the Combustion Institute* 34 (2013) 821–829. doi:10.1016/j.proci.2012.06.180.

- [16] G. Mittal, C.-J. Sung. A Rapid Compression Machine for Chemical Kinetics Studies at Elevated Pressures and Temperatures. *Combustion Science and Technology* 179 (2007) 497–530. doi:10.1080/00102200600671898.
- [17] G. Mittal, C.-J. Sung. Aerodynamics inside a rapid compression machine. *Combustion and Flame* 145 (2006) 160–180. doi:10.1016/j.combustflame.2005.10.019.
- [18] B. W. Weber, C.-J. Sung. UConnRCMPy: Python-based Data Analysis for Rapid Compression Machines. in: S. Benthall, S. Rostrup (Eds.), *Proceedings of the 15th Python in Science Conference*, pp. 36–44. http://conference.scipy.org/proceedings/scipy2016/bryan_weber.html.
- [19] B. W. Weber, R. Fang, C.-J. Sung. UConnRCMPy, 2017. v3.0.5. doi:10.5281/zenodo.815569.
- [20] D. G. Goodwin, H. K. Moffat, R. L. Speth. Cantera: An Object-oriented Software Toolkit for Chemical Kinetics, Thermodynamics, and Transport Processes, 2017. v2.3.0. doi:10.5281/zenodo.170284.
- [21] S. van der Walt, S. C. Colbert, G. Varoquaux. The NumPy Array: A Structure for Efficient Numerical Computation. *Computing in Science & Engineering* 13 (2011) 22–30. doi:10.1109/MCSE.2011.37.
- [22] E. Jones, T. Oliphant, P. Peterson, et al. SciPy: Open source scientific tools for Python, 2001–. <https://scipy.org>.
- [23] J. D. Hunter. Matplotlib: A 2D Graphics Environment. *Computing in Science & Engineering* 9 (2007) 90–95. doi:10.1109/MCSE.2007.55.
- [24] D. Lee, S. Hochgreb. Rapid Compression Machines: Heat Transfer and Suppression of Corner Vortex. *Combustion and Flame* 114 (1998) 531–545. doi:10.1016/S0010-2180(97)00327-1.
- [25] B. W. Weber, K. Kumar, Y. Zhang, C.-J. Sung. Autoignition of n-butanol at elevated pressure and low-to-intermediate temperature 158 (???) 809–819. doi:10.1016/j.combustflame.2011.02.005.

- [26] K. Kumar, G. Mittal, C.-J. Sung. Autoignition of n-decane under elevated pressure and low-to-intermediate temperature conditions 156 (2009) 1278–1288. doi:10.1016/j.combustflame.2009.01.009.
- [27] A. K. Das, C.-J. Sung, Y. Zhang, G. Mittal. Ignition delay study of moist hydrogen/oxidizer mixtures using a rapid compression machine 37 (2012) 6901–6911. doi:10.1016/j.ijhydene.2012.01.111.
- [28] J. Ortega, F. Espiau, J. Tojo, J. Canosa, A. Rodríguez. Isobaric Vapor-Liquid Equilibria and Excess Properties for the Binary Systems of Methyl Esters + Heptane. *Journal of Chemical & Engineering Data* 48 (2003) 1183–1190. doi:10.1021/jc030117d.
- [29] A. G. Camacho, J. M. Moll, S. Canzonieri, M. A. Postigo. Vapor-Liquid Equilibrium Data for the Binary Methyl Esters (Butyrate, Pentanoate, and Hexanoate) (1) + Propanenitrile (2) Systems at 93.32 kPa. *Journal of Chemical & Engineering Data* 52 (2007) 871–875. doi:10.1021/jc060469v.
- [30] R. M. Stephenson, S. Malanowski, D. Ambrose, *Handbook of the Thermodynamics of Organic Compounds*, Elsevier, New York, 1987.
- [31] A. C. van Genderen, J. van Miltenburg, J. G. Blok, M. J. van Bommel, P. J. van Ekeren, G. J. van den Berg, H. A. Oonk. Liquid–vapour equilibria of the methyl esters of alkanolic acids: Vapour pressures as a function of temperature and standard thermodynamic function changes. *Fluid Phase Equilibria* 202 (2002) 109–120. doi:10.1016/S0378-3812(02)00097-3.
- [32] S. P. Verevkin, V. N. Emel’yanenko. Transpiration method: Vapor pressures and enthalpies of vaporization of some low-boiling esters. *Fluid Phase Equilibria* 266 (2008) 64–75. doi:10.1016/j.fluid.2008.02.001.
- [33] E. E. Dames, A. S. Rosen, B. W. Weber, C. W. Gao, C.-J. Sung, W. H. Green. A detailed combined experimental and theoretical study on dimethyl ether/propane blended oxidation. *Combustion and Flame* 168 (2016) 310–330. doi:10.1016/j.combustflame.2016.02.021.

- [34] A. C. Hindmarsh, P. N. Brown, K. E. Grant, S. L. Lee, R. Serban, D. E. Shumaker, C. S. Woodward. SUNDIALS: Suite of nonlinear and differential/algebraic equation solvers. *ACM Transactions on Mathematical Software* 31 (2005) 363–396. doi:10.1145/1089014.1089020.
- [35] S. C. Chapra, R. P. Canale, *Numerical Methods for Engineers*, McGraw-Hill Higher Education, Boston, 6th ed edition, 2010.
- [36] B. W. Weber, K. E. Niemeyer. ChemKED: A human- and machine-readable data standard for chemical kinetics experiments. Submitted to: *International Journal of Chemical Kinetics* (2017). [arXiv:1706.01987](#).
- [37] J. W. Allen, C. F. Goldsmith, W. H. Green. Automatic estimation of pressure-dependent rate coefficients. *Physical Chemistry Chemical Physics* 14 (2012) 1131–1155. doi:10.1039/c1cp22765c.
- [38] B. W. Weber, C.-J. Sung, M. W. Renfro. On the uncertainty of temperature estimation in a rapid compression machine. *Combustion and Flame* 162 (2015) 2518–2528. doi:10.1016/j.combustflame.2015.03.001.
- [39] G. Kukkadapu, K. Kumar, C.-J. Sung, M. Mehl, W. J. Pitz. Experimental and surrogate modeling study of gasoline ignition in a rapid compression machine. *Combustion and Flame* 159 (2012) 3066–3078. doi:10.1016/j.combustflame.2012.05.008.
- [40] M. Ribaucour, R. Minetti, L. R. Sochet. Autoignition of n-pentane and 1-pentene: Experimental data and kinetic modeling. *Symposium (International) on Combustion* 27 (1998) 345–351. doi:10.1016/S0082-0784(98)80422-0.
- [41] J. Bugler, K. P. Somers, E. J. Silke, H. J. Curran. Revisiting the Kinetics and Thermodynamics of the Low-Temperature Oxidation Pathways of Alkanes: A Case Study of the Three Pentane Isomers. *The Journal of Physical Chemistry A* 119 (2015) 7510–7527. doi:10.1021/acs.jpca.5b00837.

- 612 [42] K. A. Heufer, J. Bugler, H. J. Curran. A comparison of longer alkane
613 and alcohol ignition including new experimental results for n-pentanol and
614 n-hexanol. *Proceedings of the Combustion Institute* 34 (2013) 511–518.
615 doi:10.1016/j.proci.2012.05.103.
- 616 [43] E. R. Ritter, J. W. Bozzelli. THERM: Thermodynamic property estimation
617 for gas phase radicals and molecules. *International Journal of Chemical*
618 *Kinetics* 23 (1991) 767–778. doi:10.1002/kin.550230903.

Ignition Delay Summary

[Click here to download Supplementary Material: complete-data-set.csv](#)

RMG Output Cantera Format

[Click here to download Supplementary Material: chem_rmg_cantera.cti](#)

RMG Output Chemkin Format

[Click here to download Supplementary Material: chem_rmg_chemkin.inp](#)

Vapor Pressure Data - Ortega et al.
[Click here to download Supplementary Material: ortega.csv](#)

Vapor Pressure Data - van Genderen et al.
[Click here to download Supplementary Material: vanGenderen.csv](#)

Vapor Pressure Code

[Click here to download Supplementary Material: vapor_pressure_fit.py](#)

Vapor Pressure Data - Verevkin et al.
[Click here to download Supplementary Material: verevkin.csv](#)

RMG Input File

[Click here to download Supplementary Material: rmg_input.py](#)

LaTeX Source Files

[Click here to download LaTeX Source Files: methyl-valerate.zip](#)